공학석사학위논문

가솔린 엔진에서의 0-D 노킹 발생예측 모델링에 관한 연구

A Study on 0-D Knock Prediction Model in a Spark-ignited Engine

2019 년 2 월

서울대학교 대학원

기계항공공학부

송 치 헌

Acknowledgement

First and foremost, I would like to express my respect and sincere appreciation to my adviser, Professor Kyoungdoug Min for providing inspiration and encouragement. As a professor, he has shown me not only what research is like, but also how to elevate and take care of the members as a leader. Without his support, this accomplishment would not have been possible. I extend my gratitude to Seoul National University and the professors in the committee, Professor Seung Hawn, Ko and professor Han Ho, Song for their comments on my research topic.

A special thanks goes to Dr. Seokwon Cho for his valuable advice and pleasant discussion. I could learn a lot of things from working together for two years. He has been willing to discuss and motivate me whenever I have trouble breaking through obstacles, not only in research but also in daily life.

I would like to express my deep appreciation and sorry to Youngbok Lee for his dedicated help to the modelling parts of this research. No matter how annoying I was, no matter how busy he was, he has gladly discussed on my problems. Thanks to his help, I was able to relieve many hardships in proceeding this research.

Also, I want to say thank to Sechul Oh for his willingness to be helpful for this research. His kindness always have encouraged me whenever I feel helpless and distressed. Without his encouragement, I would have felt more anxious and impatient on continuing the research.

I have to show my gratitude to all of the laboratory members. I think I am really lucky to meet all of you. Not only I met passionate researchers, but I also could get close friends. I have learnt a lot both intellectually and personally from

all of you. And, although it didn't look like that, I had a lot of fun for the last two years with you. Thank you very much for teaching me a lot and leaving me good memories. I hope everyone will do really, really well in the future.

I cannot forget to thank my old friends, Hyuntae Son, Kibeom Byun and Harin Jeon, who have spent enjoyable time and shared precious memories for 9 years since high school days. The break time with them was time for me to recharge my mind.

Lastly, I would like to present gratitude to my parents, Sunseob Song, Kyoungja Oh. Their dedication has made whom I am now. And I say thanks to my older sister, Heewon Song, for being a good friend and a warm family to me.

Abstract

A Study on 0-D Knock Prediction Model in a Spark-ignited Engine

Chiheon Song
Department of Mechanical and Aerospace Engineering
The Graduate School
Seoul National University

Though the efficiency improvements of gasoline engines have been continually studied, the recent surge in fuel efficiency and emissions regulations has made the need for greater effort on efficiency improvement than ever before. Therefore, various methods have been proposed to improve the efficiency of gasoline engines, and among them, the increase in compression ratio has been known to be effective in improving fuel efficiency. However, the higher compression ratio increases the initial temperature of the mixture, which is led to in-cylinder condition which auto-ignition is likely to occur.

If auto-ignition occurs in the form of an explosion, a stiff heat release occurs and forms a pressure wave inside the cylinder, causing noise and engine damage. This is called a knock and must be avoided to prevent engine damage. Therefore, various control algorithms have been proposed to avoid knock as well as researches to mitigate knock.

Knocking control algorithms in conventional mass-produced vehicles rely on knock sensors. Because it is preceded by detection of knock from sensors, knock cannot be completely avoided. In addition, the control parameters change rapidly

to avoid convolutions in case of knock, which not only deteriorates the driving convenience but also decreases fuel efficiency In order to improve this point, progressive control methods are being developed.

The knock phenomenon is influenced by factors such as gas flow, heat transfer and combustion characteristics in the engine, so that it shows random characteristics. Therefore, in order to avoid the knocking conservatively, the conventional control slowly returns the operating parameters to the optimum condition after knocking avoidance. This maintains the operating conditions at lower efficiency points, so additional efficiency improvement is expected in high load condition if the control algorithm is improved.

As one of the solutions, an advanced control with knock prediction can be suggested. In this case, not only is it able to avoid knock, but also by determining control factors prior to knock occurrence, it is also possible to avoid efficiency deterioration due to excessive change in control parameters.

In this study, modeling of knock prediction was done as a base study for model based control. In the model, only operating parameters and measured values obtainable from the mass production engine were used, considering the application to actual driving conditions. Firstly, the in-cylinder pressure prediction modeling was done with three steps; determination of the initial conditions inside the cylinder, pressure prediction during the compression, and combustion pressure prediction using the burn rate. Additionally, with consideration on variation of Wiebe function, the cyclic variation model was constructed.

Secondly, the temperature of the unburned gas was calculated using the predicted pressure. With those value, the ignition delay was calculated. Since the ignition delay only determines the onset of auto-ignition, not the occurrence, the burn rate at predicted onset was used to determine the knock occurrence.

The pressure prediction and ignition delay model were combined to a single model and tested with cyclic variation model. As a result, the model was judged to have sufficient accuracy, predicting knock incidence accurately under various operating conditions.

Keywords: Spark-ignited engine, Knock prediction, In-cylinder pressure prediction, Auto-ignition, Ignition delay.

Student Number: 2017-29399

Contents

List of Tables

List of Figures

Nomenclature

A	area [m^2]
CA	crank angle [deg]
CR	compression ratio [-]
E_a	activation energy [J]
h_w	convective heat transfer coefficient [$W\ m^{-2}\ K^{-1}$]
k	polytropic coefficient [-]
k_B	Boltzmann constant [$J\ K^{-1}$]
k_{Arr}	rate constant
m	mass [kg]
MFB	mass fraction burned [-]
N	number [-]
n	mole number [-]
P	pressure [bar]
Q	heat [J]
Q_{LHV}	low heating value [$J\ kg^{-1}$]
R	ideal gas constant [$J\ mol^{-1}\ K^{-1}$]
R_s	specific ideal gas constant [$J\ kg^{-1}\ K^{-1}$]
S_p	piston speed [$m\ s^{-1}$]
T	temperature [K]
t	time [s]
t_{IGN}	ignition time [s]
V	volume [m^3]

Greek Letters

γ	specific heat ratio [-]
θ_b	burn duration [deg]

η	efficiency [-]
λ	stoichiometric ratio [-]
ρ	gas density [kg m^{-3}]
τ	ignition delay time [ms]

Subscripts/Superscripts

a	air
b	burned zone
c	combustion
chem	chemical
eff	effective
f	fuel
HT	heat transfer
ign	ignition
in	intake
n	net
p	piston
r	residual
stoi	stoichiometric
u	unburned

Acronyms

0D	zero-dimensional
1D	one-dimensional
3D	three-dimensional
aBDC	after bottom dead center
AEFD	average energy of pressure oscillation in frequency domain
AHHR	accumulated heat release rate
aTDC	after top dead center

bBDC	before bottom dead center
BDC	bottom dead center
bTDC	before top dead center
CA	crank angle
CA10	crank angle at mass fraction burned 10 %
CA50	crank angle at mass fraction burned 50 %
CA90	crank angle at mass fraction burned 90 %
CFD	computational fluid dynamics
CI	compression ignition
CVVT	continuous variable valve timing
DKI	dimensionless knock indicator
ECU	engine control unit
EGR	exhaust gas recirculation
EMS	engine management systems
EOC	end of combustion
EV	electric vehicle
FFT	fast Fourier transform
GDI	gasoline direct injection
HEV	hybrid electric vehicle
HRR	heat release rate
IMEP	indicated mean effective pressure
ISPO	integral of squared pressure oscillation
IMPO	integral of modulus of pressure oscillation
IVC	intake valve closing
KI	knock intensity
KLSA	knock limit spark advance
LHV	low heating value
LKI	logarithmic knock intensity
MAPO	maximum amplitude of pressure oscillation

MBT	maximum brake torque
MFB50	mass fraction burned 50 %
NEDC	new European driving cycle
ON	octane number
PFI	port fuel injection
PHEV	plug-in hybrid electric vehicle
PRF	primary reference fuel
PSD	power spectral density
RCEM	rapid compression-expansion machine
RDE	real driving emission
RGF	residual gas fraction
RMSE	root mean square error
RON	research octane number
RPM	revolution per minute
SEPO	signal energy of pressure oscillation
SOC	start of combustion
SOI	start of injection
TDC	top dead center
TVE	threshold value exceed

Chapter 1. Introduction

1.1 Backgrounds and Motivations

The increasing concerns on the global warming and air pollution have been leading to more stringent regulation on exhaust gas emission from vehicles. In this situation, for CO2, European Union have set the regulation to be 95 g/km of CO2 emission by 2021 and 67 g/km by 2030 [1]. This trend of emission regulation requires 5 % of reduction of CO2 emission annually. Following this initiative of European Union, CO2 regulation of many governments also requires similar level of emission. United States government requires 99 g/km of CO2 regulation by 2025, which is same level of that of Canada. For South Korea, the government also enforces the CO2 emission to be 97g/km by 2020. Furthermore, due to the gap between official and real-world emission, the harsher emission testing procedures such as WLTP and RDE test are becoming widely applied.

In this situation, the carmakers are increasing the sales potion of the battery electric vehicles (BEV) and the fuel cell electric vehicles (FCEV). However, the market share of the vehicles with internal combustion engine, including hybrid electric vehicles (HEV), is still dominant around the world in 2017 [1] and this trend is predicted to be continued. The future market share of internal combustion engine is predicted to be more than 80 % in 2030, when including hybrid electric vehicles [2, 3, 4]. At the same time, due to the public perception on the emissions from diesel engine, the market share of diesel vehicles are declining and predicted to be minor powertrain on light duty vehicle while the total number of cars is increasing [2, 5, 6]. Therefore, improvement on fuel efficiency in gasoline engines becomes important more than ever.

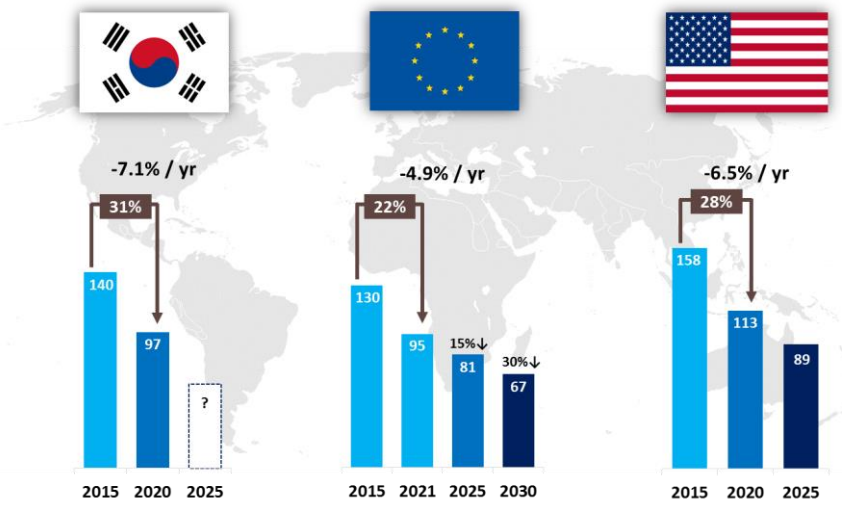

Figure 1.1 Global trend of CO2 regulation [1]

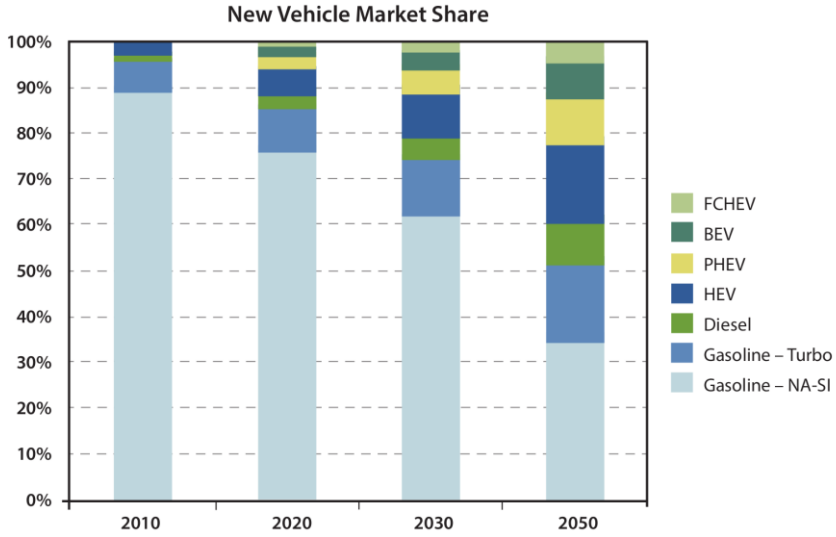

Figure 1.2 Prediction for market share of powertrain system [4]

The efficiency of an internal combustion engine can be mainly analyzed in four aspects: combustion efficiency, thermal efficiency, pumping loss and friction. The combustion efficiency is about conversion efficiency of chemical energy to heat energy while the thermal efficiency means conversion of heat energy to mechanical energy. Both are generally multiplied and evaluated in terms of fuel conversion efficiency. Pumping loss is amount of work which is generated during gas exchange process due to pressure difference between intake and exhaust stroke. In the last, and friction is from relative motion of various mechanical parts.

To achieve desired torque and power while reducing fuel consumption, minimizing those energy loss is important. Thus, a bunch of technologies has been introduced on gasoline engines. To improve fuel conversion efficiency, advanced injection strategies such as multi-point injection (MPI), gasoline direct injection (GDI) and open valve injection (OVI) are on research and application. Furthermore, to reduce pumping loss and adjust effective compression / expansion ratio, variable valve systems including continuous variable valve timing (CVVT) and lift (CVVL) also have been applied. However, although these state-of-art technologies have been applied, the direct and effective way is to increase compression ratio which is traditionally known.

It is well known that the high compression ratio can ensure high thermal efficiency of an internal combustion engine due to its characteristic as a heat engine [7]. Its thermodynamic relationship is expressed in equation 1.1.

$$\eta = 1 - \frac{1}{CR^{k-1}} \tag{1.1}$$

However, in case of spark-ignited engine, it is difficult to apply the high compression ratio due to knock phenomenon.

Knock is a kind of auto-ignition phenomenon that occurs in the unburned gas region during combustion. As combustion proceeds, in-cylinder pressure increases so that unburned gas region is compressed and its temperature increases. If the flame does not reach unburned gas region before ignition delay is over, than auto-ignition occurs. When the auto-ignition occurs in form of detonation, rapid heat release and pressure rise are generated. The example knocking pressure trace is depicted in figure 1.3. This stiff heat release and pressure wave are known to cause not only noise but also erosion on mechanical components, leading to engine failure [8, 9, 10, 11]. Therefore, knock occurrence must be avoided during engine operation.

Generally, to operate SI engine with high fuel efficiency as possible, spark timing should be kept at maximum brake torque (MBT) timing. However, advancing spark timing under high load condition also causes knock-prone state in cylinder by increasing pressure and temperature. Thus, knock avoidance of the conventional SI engines is realized by retarding the spark timing when knock is detected with the knock sensor. Majority of conventional spark control logics have employed fast retardation and slow advance to ensure engine safety [12, 13, 14]. However, this strategy keeps the spark timing to be slightly more retarded from knock limit spark timing (KLSA) which deteriorates the fuel efficiency [15]. Therefore, continuous effort on knock control improvement is ongoing.

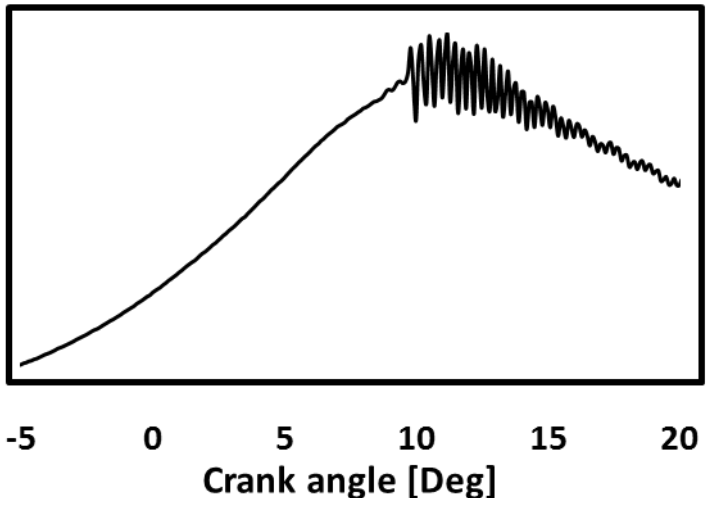

Figure 1.3 Pressure trace of knocking cycle

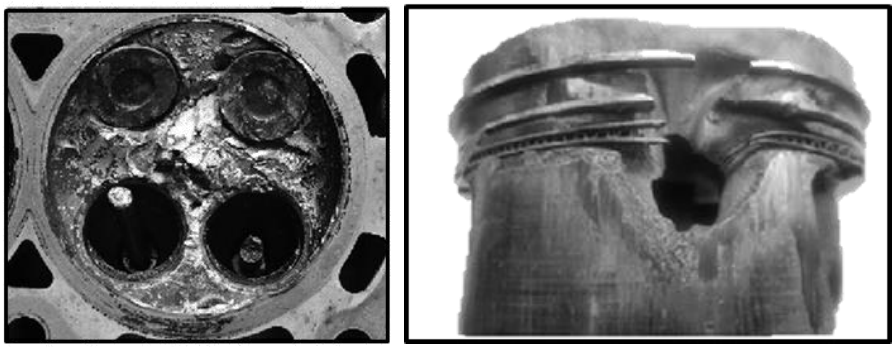

Figure 1.4 Damage on engine parts by knock [11]

1.2 Literature Review

1.2.1 Auto-ignition and knock phenomenon

Knock phenomenon is generated by auto-ignition of unburned air-fuel mixture, followed by strong pressure wave in cylinder. Thus, not does every mode of auto-ignition cause the damage on engine. Combustion modes can be classified in two major form; deflagration and detonation [16]. When the auto-ignition occurs as deflagration in combustion chamber, it hardly induce noise and damage on the engine because the combustion wave propagates slower than sound speed and cannot generate strong pressure wave. On the contrary, because the detonation wave propagates with faster velocity than sound speed, detonation mode of auto-ignition can causes pressure wave in the engine, leading to noise and damage [17, 18].

The auto-ignition is considered to be initiated when the concentration of radical species reaches critical value. Therefore, the ignition delay of air-fuel mixture is largely affected by its composition, the pressure and temperature history. It is expressed in equation 1.2. x* is pertinent reaction products and τ is empirical function for ignition delay.

$$\frac{dx^*}{dt} = \tau(P, T, t, \lambda, Composition, \text{etc.}) \quad (1.2)$$

Although the auto-ignition is not sufficient condition, it is critical necessary condition for knock occurrence. Therefore, researches on engine knock generally considers the end of ignition delay as knock onset [19, 20, 21]. Unlike the conventional auto-ignition research with RCEM, auto-ignition in knock research

goes through much transient condition. Thus, in knock researches, Livengood-Wu integral [22] is often used to estimate the ignition delay. The correlation is shown in equation 1.3. x_c is a critical concentration of pertinent reaction product.

$$\frac{(x^*)}{(x_c)} = I = \int_{t=0}^{t=t_{IGN}} \frac{1}{\tau} dt \tag{1.3}$$

If the I value reaches unity, it means that the concentration of radical element is enough to initiate auto-ignition.

To understand the correlation between these parameters and ignition delay, numerous empirical models for ignition delay have been established by using the rapid compression-expansion machine (RCEM) [22, 23, 24]. Majority of these models have form of Arrhenius equation as equation 1.4, which is based on activation of chemical reaction. A is collision frequency which is variant for each chemical reaction.

$$k_{Arr} = A * exp(-\frac{E_a}{k_B T}) \tag{1.4}$$

Douaud and Eyzat [19] introduced an ignition delay model, which is based on chemical reaction and considering octane number of fuel. The formula is as expressed in equation 1.5. Coefficients of model were calibrated with experimental data using the CFR engine. Considering various octane number, various composition of primary reference fuel (PRF) was determined.

$$\tau = 18.69 \left(\frac{ON}{100}\right)^{3.4017} P^{1.7} \exp(\frac{3800}{T}) \tag{1.5}$$

Worret et al. [25] modified the Douaud-Eyzat model by conducting experiment with conventional engine and two types of fuel with different research

octane number (RON). They suggested that the term of octane number in Douaud-Eyzat model can be replaced to RON with same model coefficients.

Hoepke et al. [26] investigated the effect of cooled EGR on knock as boosting and downsizing strategies had been applied. They analyzed that the effect of EGR on knock mitigation is majorly appears in three aspects; burn rate improvement, chemistry change and increase of specific heat ratio. Among these factors, the effect of burn rate and specific heat ratio appears as change of in-cylinder pressure and unburned gas temperature. For the chemistry change, they introduced additional term with EGR to lengthen ignition delay. Furthermore, density of gas is considered, not pressure solely as existing model. The derived model is as followed in equation 1.6.

$$\tau = 8.4498 * 10^{-5} \left(\frac{\mathrm{P}}{\mathrm{T}}\right)^{-1.343} (1 - x_{EGR})^{-0.8881} \exp\left(\frac{5266}{T}\right) \qquad (1.6)$$

Chen et al. [20] compared existing ignition delay models and found that the existing models were vulnerable to change of air/fuel ratio in the engine. It is analyzed that the excessive oxygen in the air affects not only pressure and temperature but chemical reaction. Therefore, an explicit term with stoichiometric ratio (λ) is additionally included to Hoepke's model as equation 1.7.

$$\tau = 5.35 * 10^{-5} \left(\frac{\mathrm{P}}{\mathrm{T}}\right)^{-2.374} (1 - x_{EGR})^{-3.013} \lambda^{-1.927} \exp\left(\frac{3167}{T}\right) \qquad (1.7)$$

Recently, Mckenzie et al. [27] improved ignition delay model with consideration on various types of dilute gas including EGR, residual gas and excessive air. In this model, the effect of dilute gases is combined as one explicit term. The model has formula as expressed in equation 1.8.

$$\tau = 2.71 * 10^{-5} \left(\frac{\mathrm{P}}{\mathrm{T}}\right)^{-1.73} \exp\left(\frac{5190}{\mathrm{T}}\right)(1 - \mathrm{W_d})^{-0.618}$$

$$\mathrm{W_d} = \mathrm{EGR} + \mathrm{x_r} + 0.95\left|\frac{\lambda - 1}{\lambda + \mathrm{A/F_{Stoi.}}}\right| \quad (1.8)$$

Cho [28] induced the formula to understand the ignition delay considering molar concentration of each element. The formula was induced based on a chemical reaction rate as in equation 1.9. The fuel and oxygen concentration was regressed with gas density and equivalent ratio. The regression is expressed in equation 1.10 and equation 1.11. These two equation was substituted to equation 1.9 and calibrated, resulting in equation 1.12.

$$r = A[Fuel]^m[O_2]^n exp(-\frac{E_a}{RT}) \quad (1.9)$$

$$x_f = \frac{n_f}{n_{fuel} + n_{air} + n_r + n_{egr}} \sim \frac{C}{\lambda} \quad (1.10)$$

$$x_{O_2} = \frac{n_a}{n_f + n_a + n_r + n_{egr}} \approx C \quad (1.11)$$

$$\tau = 3.255 * 10^{-5} \left(\frac{\mathrm{P}}{\mathrm{T}}\right)^{-2.183} \lambda^{-0.4408} \exp(\frac{3318}{T}) \quad (1.12)$$

1.2.2 Knock methodologies

1.2.2.1 Evaluation of knock intensity

Detection of knock occurrence is one of the most important part not only in actual engine operation but also in knock research. Generally, in the field of knock research, knock occurrence is judged on the basis of the strength of knock, which is called as knock intensity. Therefore, various methodologies to define strength of knock have been developed. Majority of these methodologies are based on the measured in-cylinder pressure because the knock occurrence generally accompanies with pressure oscillation.

Among various knock metrics using the pressure data, the MAPO (maximum amplitude of pressure oscillation), IMPO (integral of modulus of pressure oscillation) and ISPO (integral of squared pressure oscillation) are the representatives. For MAPO, it uses high pass filtered pressure signal and defines knock intensity as maximum amplitude of filtered signal. Due to its simplicity and intuitiveness, it has been widely applied to knock research [18, 26, 28, 29, 30]. However, because MAPO method uses only one data point, it shows vulnerability on external noise. IMPO evaluates knock intensity by summing amplitude of filtered pressure signal. Similarly, ISPO evaluates knock intensity by summing squared amplitude of filtered pressure signal. Both IMPO and ISPO methods consider energy of signal but, difficulty exists on determining the calculation duration, which can lead to a bias on evaluation.

Therefore, researches for standardization of knock intensity have been conducted. For example, AEFD (average energy in the frequency domain) was introduced to minimize dependency on calculation duration [31]. This method

evaluates knock intensity in the same way as ISPO but with the spectral lines obtained by Fourier transform.

Hudson et al. [32] suggested LKI (logarithmic knock intensity) with consideration on oscillation energy in the frequency domain. This method calculates knock intensity by taking logarithm on averaged energy. They verified LKI method in both time domain (averaged ISPO) and frequency domain (AEFD).

Brecq et al. [33] introduced the DKI (dimensionless knock indicator) to determine knock limit of an engine. The DKI is defined as the ratio of IMPO and MAPO value multiplied by calculation window, which means the ratio of swept area by each method. They found that DKI value sharply decreased when spark timing was advanced beyond knock limit spark timing (KLSA).

Shahlari et al. [34] developed knock intensity based on envelope of pressure oscillation history. This method creates signal envelop on high pass filtered pressure in form of exponential and defines the pre-exponential constant (K) as knock intensity. They concluded that this developed method had less dependency on position of pressure transducer than existing methods did.

Cho [28] defined knock incidence as a number of knocking cycles divided by total number of cycles. Considering the stochastic behavior of knock, at least 1000 of cycles were monitored to have statistical validity. They found that the knock incidence had strong positive correlation with ISPO knock intensity. Therefore, they concluded that the knock incidence also can be a representative index for knock intensity without complex arithmetic calculation.

Table 1.1 Knock intensity metrics

MAPO	Maximum Amplitude of Pressure Oscillation	$\max(\lvert P_{filt} \rvert)$
IMPO	Integral of the Modulus of Pressure Oscillation	$\int_{\theta_0}^{\theta_0+\Delta\theta} \lvert P_{filt} \rvert d\theta$
ISPO	Integral of Squared Pressure Oscillation	$\int_{\theta_0}^{\theta_0+\Delta\theta} {P_{filt}}^2 d\theta$
AEFD	Average Energy of pressure oscillation in Frequency Domain	$\int_{\nu}^{\nu+\Delta\nu} [\mathcal{F}(P)]^2 \, d\nu$
LKI	Logarithmic Knock Intensity	$\ln(C \times$ averged ISPO$)$ (or $\ln(C \times$ AEFD$)$)
DKI	Dimensionless Knock Intensity	$\frac{\text{IMPO}}{MAPO * L_{Window}}$
Sharlari	Signal Enveloping Method	$\mathrm{K} = \mathrm{K}_0 e^{-mt}$ $\mathrm{K}_0 = knock\ intensity$
Knock incidence	Frequency of knock occurrence	$\frac{\mathrm{N}_{\text{knocking cycle}}}{\mathrm{N}_{\text{monitored cycle}}}$

1.2.2.2 Knock onset determination

Determination of knock onset is another critical factor in the field of knock research because incorrect estimation of knock onset timing leads to misunderstand on anatomy of knock and ignition delay of fuel. Because knock phenomena generally appears with pressure oscillation, knock onset can be determined by detecting the beginning of pressure oscillation. However, due to the stochastic behavior of knock, analysis of knock requires numerous amount of pressure trace, which makes it difficult capture the knock onset manually. Therefore, researchers have developed knock onset detection algorithms.

One of the conventional methods is MAPO-TVE (MAPO-threshold value exceed) method. This method processes the pressure signal in the same way of MAPO method and defines knock onset as when the amplitude of oscillation exceeds a threshold value. As MAPO method does, this method has its priority on simplicity and intuitiveness. However, this method has tendency to detect knock onset later than knock actually occurs.[25, 35].

Kim [36] introduced modified TVE method to improve the MAPO-TVE method. They filtered the pressure signal by subtracting smoothed signal from raw signal to minimize phase shifting by conventional filtering. After signal processing, algorithm detects the first dip of oscillation. From 5 degrees before the first dip, it monitors the mean and standard deviation of filtered pressure signal in moving window. If the pressure oscillation exceeds sum of average and five times of standard deviation, previous crank angle is determined as knock onset.

Khalghatgi et al. [29] determined knock onset with smoothed pressure signal. The moving average with window length of 3 is used for pressure smoothing. This algorithm defines knock onset as when the difference of smoothed pressure data

exceeds 0.05 bar. The determined knock onset with developed algorithm was compared with manually observed onset, showing high coincidence.

Shahlari et al. [34] used raw pressure signal to determine knock onset. With proper initial guess on knock onset, this algorithm conducts a linear fitting on pressure data with weight. If the difference between raw pressure and fitted line exceeds 0.1bar, than that crank angle becomes new initial condition. After repeating this procedure five times, knock onset is determined.

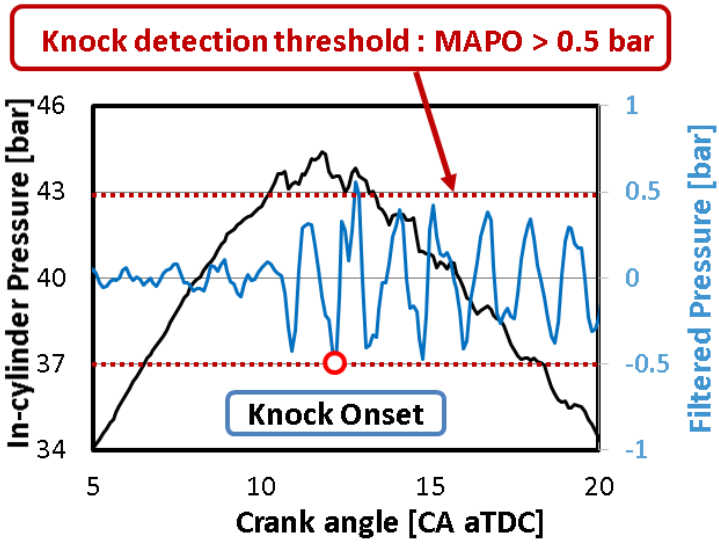

Figure 1.5 MAPO-TVE method

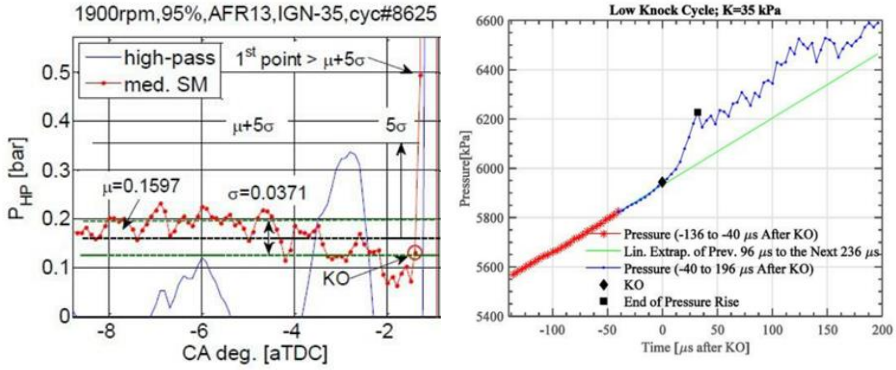

Figure 1.6 Advanced TVE method (left) and Sharlari's method(right)

1.2.3 Knock mitigation strategies

1.2.3.1 Coolant strategy optimization

Suppression of temperature rise has significant effect on knock mitigation because the auto-ignition is governed by temperature of unburned gas mixture. Therefore, majority of conventional knock mitigation researches are related to gas temperature. For example, application of EGR is one of certain methods to reduce temperature rise by increasing specific heat ratio of mixture [26]. Thus, it have been actively applied to the mass-production engines [37, 38, 39].

Optimizing coolant strategy is one of promising factor on knock mitigation because it has direct effect on boundary temperature of the cylinder. However, excessive cooling can increase heat transfer between burned gas and boundary wall, which can lead to deterioration of thermal efficiency. Therefore, numerous researches for optimizing cooling strategy have been conducted. Optimization of coolant passage and piston oil gallery are widely on application for mass-production engines [40, 41].

Takahashi et al.[42] studied the effect of a liner temperature distribution with experiment and 3D CFD simulation. They analyzed the heat transfer characteristics along each period of engine cycle. Due to the change of effective liner area during cycle, the heat transfer through liner was largest during gas exchange process while being smallest during combustion process. Furthermore, tumble motion of intake flow resulted in the larger effect of exhaust side wall.

Imaoka et al.[43] analyzed the effect of each wall on knock mitigation by applying segregated cooling passage on the engine. The CFD simulation result showed that the majority of heat transfer occurred through the intake port and

valve surface. In addition, experiment result showed that cooling the head coolant had larger effect on knock mitigation, consistent with the CFD analysis. Furthermore, they adopted the insulated intake port to the test engine to decrease initial gas temperature for knock mitigation.

Cho [28] investigated the effect of coolant on each wall temperature and knock mitigation. The CFD analysis result showed that the cooling strategy did not have considerable effect during combustion due to small change of wall temperature compared to burned gas temperature. They pointed out that the effect of head coolant on knock mitigation mainly came from the intake port wall, not the head surface. Furthermore, it appeared that the liner cooling could be more effective with the insulated intake port.

1.2.3.1 Improvement of flame propagation

Flame propagation is another important factor because it governs the existence of unburned gas at the end of ignition delay. Although knock mitigation with flame speed improvement requires delicate consideration on combustion, this strategy brings not only knock mitigation but also efficiency improvement. Therefore, some concepts including corona ignition [44, 45] and multi ignition [46, 47] have been introduced for faster and larger kernel growth at start of combustion.

On the other hand, increasing turbulent intensity at the spark timing is known to be another solution for improving flame propagation, by expanding flame surface area [16]. In case of the SI engine, it is traditionally accepted that the higher tumble ratio ensures the stronger turbulent intensity at the spark timing. Thus, researches for improving in-cylinder flow characteristics have been conducted and applied to the engine design.

Recently, Yoshihara et al. [48] published design procedure of high tumble port. They pointed out that the improvement on tumble ratio led to decrease of flow coefficient, resulting low volumetric efficiency. Therefore, design related to valve seat was optimized to suppress flow coefficient deterioration. The intake port was inclined to lead the gas flow into one direction on the valve curtain area.

Omura et al. [49] equipped the laser Doppler velocimetry system on the test engine to measure the turbulent intensity. Various flow condition was tested by using intake port adapter. Result showed that the turbulent intensity and mean flow velocity near spark timing tended to increase as tumble ratio increase. It was analyzed due to the vortex center with high tumble moved to spark more than it did under low tumble condition.

1.2.3.1 Retarding the spark timing

Knock phenomena shows stochastic behavior due to the variation of numerous factors such as air-fuel mixing, turbulent flow, residual gas and flame growth. Therefore, despite the efforts on knock mitigation, it is still difficult to guarantee knock-free operation under specific condition. In order to avoid knock, conventional vehicles are using real-time spark control algorithm.

Generally knock avoidance is realized by retarding spark timing, however, it inevitably leads to efficiency deterioration. Therefore, various spark control logic has been developed to minimize efficiency loss from retarding the spark timing. For example, Denso cooperation held a patent [50] for spark control algorithm which updates its control factors in real time.

Cho et al. [51] developed the spark control algorithm with consideration on cyclic variation. In order to establish the environment for model development, a simulation model for in-cylinder pressure was constructed considering cyclic

variation. They found that the location of peak pressure had major effect on combustion phase and knock occurrence. Therefore, the peak pressure location was determined as a factor for tuning the control gain. The model was validated by experiment and showed less fluctuation of spark timing.

Thomasson et al. [15] introduced a control algorithm based on likely-hood of knock incidence under various operating condition. They varied the spark timing with fixed intake pressure to observe the correlation between the knock incidence and the spark advance. The observed likely-hood was applied to change the control gain in real time to achieve less the variation of spark timing compared to conventional strategy. The experiment result with the developed control logic showed not only smaller variation of spark timing but also lower probability of knock occurrence.

1.3 Research objective

Not only knock prediction is an important challenge for the active knock avoidance, but also it can be a basis for the utilization of auto-ignition to achieve the fast combustion. Knock related control is typically realized by adjusting the spark timing. Therefore, it is important to complete the knock prediction before the spark is discharged for progressive spark control.

While there have been numerous researches on knock prediction models, these models are difficult to apply in actual driving situations because of a gap between the real situation and model requirements such as in-cylinder pressure sensor, long calculation time or other unavailable data in real situation. Thus, the research objective was development of a 0-D knock prediction model with only available data from the engine management system. To achieve the objectives, the following process was carried out.

1). Cycle-based combustion analysis

- Combustion process of the test engine were characterized.

2). In-cylinder pressure prediction

- A 0-D in-cylinder pressure prediction model was developed with available EMS data.

3). Determination of knock occurrence

- Criteria for knock occurrence were proposed with consideration on ignition delay and mass fraction burned.

Chapter 2. Methodology

2.1 Test cell configuration

2.1.1 Test engine specification

The test engine was a single cylinder SI engine with displacement volume was 500cc. The stroke and bore were 97mm and 81mm respectively and compression ratio was 12. The intake air was naturally aspirated and fuel was supplied with multi point injection system. This engine was equipped with the dual CVVT system, in which the intake valve could be advanced by 50CA and exhaust valve could be retarded by 40CA. The engine is shown in figure 2.1 and its detail is in table 2.1.

2.1.2 Cell facility and equipment

The schematic diagram for test cell configuration is depicted in figure 2.2. For the intake throttle and the CVVT module control, the mass production ECU was used with ETAS INCA software. For the ignition and injection control, the compact-RIO platform of National Instrument was programmed by Labview software. This system enabled to obtain the control resolution of 0.1CA with the rotary encoder of 3600 ticks. Therefore, more precise control of spark timing and injection duration was achieved.

The measured data was monitored and logged with AVL Indimodul system. Kistler 6065A piezoelectric pressure sensor was mounted in the cylinder head. The flush mounting type was selected to measure pressure oscillation accurately

while reducing the resonance in cavity as much as possible. Kistler 4045A2 absolute pressure sensor was used to measure the intake pressure. The in-cylinder pressure data was calibrated with the measure pressure at intake manifold during BDC ± 2CA in the intake process. Additionally, in-cylinder pressure was also acquired with the developed Labview program to calculate knock incidence in real time.

The fuel was supplied at the pressure of 6bar and its flow rate was monitored with OVAL CA001 Coriolis type flowmeter. The fuel was the conventional gasoline fuel, which had 42.825 MJ/kg of low heating value, 2.064 of H/C ratio and 91.5 of research octane number. The fuel specification is in table 2.2. Fuel injection duration was controlled to keep the lambda to be unity. The lambda value was monitored with Horiba MEXA-110 λ lambda analyzer.

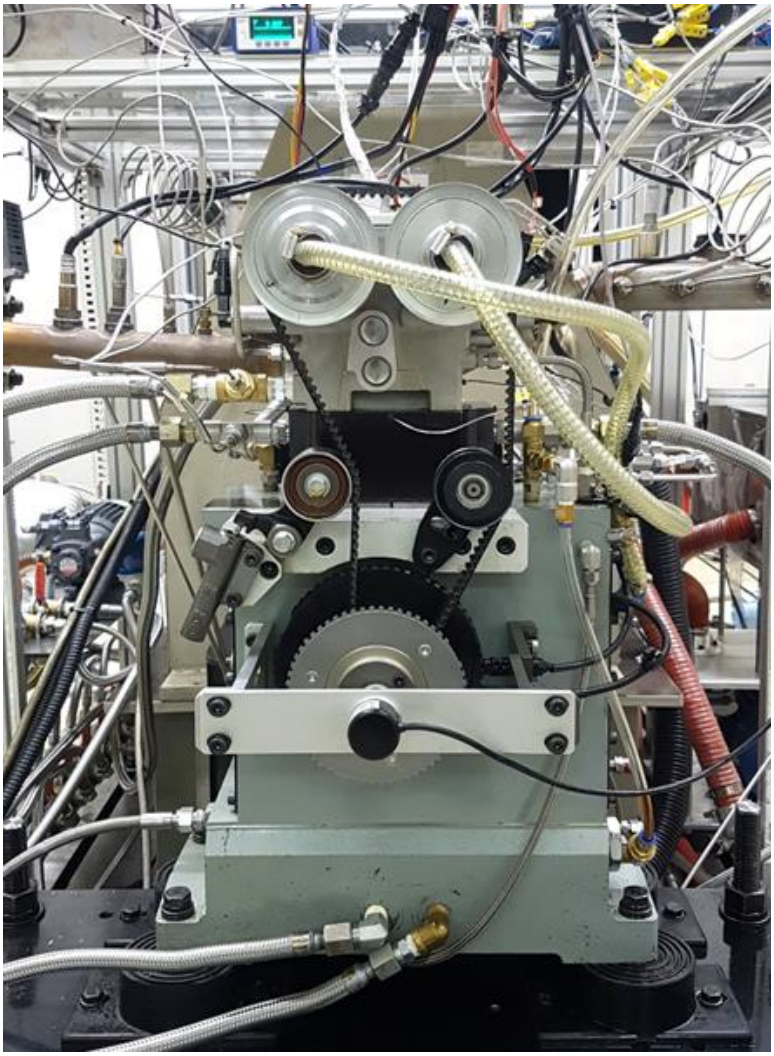

Figure 2.1 Single cylinder SI engine

Table 2.1 Engine specification

Category		**Specification**
Engine type		Single-cylinder N/A dual CVVT
Displacement [cc]		499.8
Stroke [mm]		97
Bore [mm]		81
Compression ratio		12
Injection system		Dual PFI (6 bar)
Injection timing		540 CA bTDC
Valve Timing (@ 0.1 mm)	EVO	68 CA bBDC
	EVC	1 CA aTDC
	IVO	10 CA aTDC
	IVC	67 CA aBDC
Number of valves		4
Maximum valve lift		10 mm

Table 2.2 Fuel specifications

Conventional gasoline	Value	Test Method
H/C ratio	2.064	ASTM D 5291
Density [kg/m^3] @ 15°C	724.5	ASTM D 1298
Research Octane Number	91.5	ASTM D 2699
LHV [MJ/kg]	42.825	ASTM D 240-14

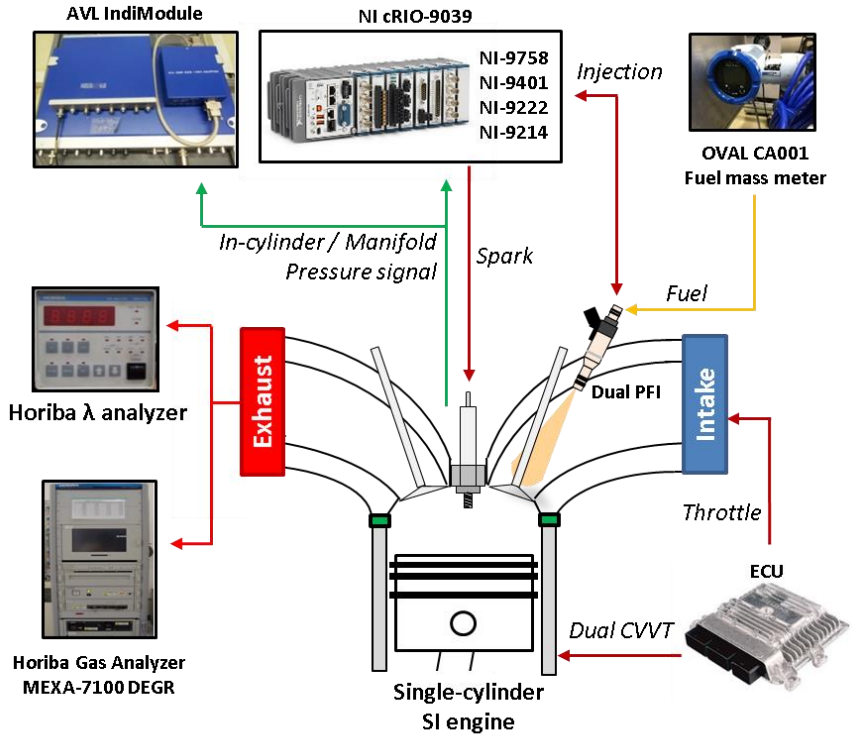

Figure 2.2 Test cell configuration

2.2 Experimental conditions

2.2.1 Knock detection and incidence

Knock detection was an important issue because the research objective was closely related to knock occurrence. In this research, the knocking cycle was determined with MAPO-TVE method. The threshold value was selected to be 0.5 bar to detect weak knock while distinguishing pressure oscillation caused by knock or signal noise. For the strength of knock, knock incidence was used to estimate the strength simply and intuitively during experiment.

2.2.2 Operating condition

The experimental conditions were determined to obtain abundant data under different knock incidence condition. Therefore, various combinations of engine load, combustion phase and valve timing were tested. The test procedure was as followed.

1. Operate the test engine on normal condition keeping MFB50 timing to be aTDC 8 CA.

2. Increase fuel rate with fixed MFB50 timing until knock incidence exceeds 50 %.

3. If knock incidence exceeds 50 %, than fix the fuel rate and retard the ignition timing until knock does not occur.

This test procedure was repeated at 1000, 1500 and 2000 rpm with various intake pressure. The valve timing was also changed; the intake valve was advanced by 0, 5, 45 CA and the exhaust valve was retarded by 0 and 5 CA. The test condition was depicted in table 2.2 and figure 2.3.

Table 2.3 Experimental condition

Valve Timing	0 - 50 CA adv. (In) 0 - 5 CA rtd. (Ex)
Spark Timing	28 CA bTDC - 4 CA aTDC
Intake Pressure [bar]	0.6 – 0.9
Engine Speed [rpm]	1000/1500/2000
Ambient Temp. [°C]	25
Oil/Coolant Temp. [°C]	85

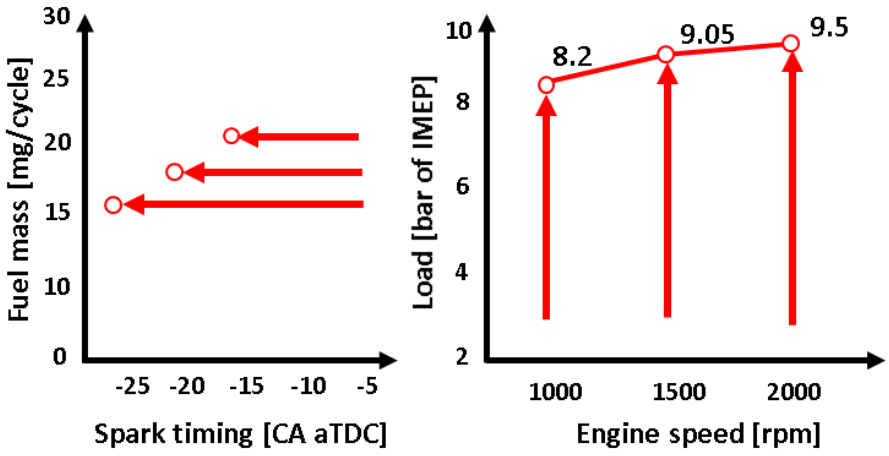

Figure 2.3 Operating region

2.3 Combustion analysis

2.3.1 Heat release rate and heat loss

Estimation of heat release rate is an important part in combustion analysis because it gives some representative parameters such as MFB50, amount of heat loss and burn duration. However, it is difficult to calculate the heat release rate accurately because the available data is usually only in-cylinder pressure. Typically, the heat release rate is calculated with the single zone assumption and 1st law of thermodynamics. The calculation is carried out as in equation 2.1.

$$dQ_{net} = \frac{\gamma}{\gamma-1} PdV + \frac{1}{\gamma-1} VdP \tag{2.1}$$

By accumulating the calculated heat release rate along crank angle, mass fraction burned can be estimated in terms of energy fraction. It is shown in equation 2.2.

$$\mathrm{x_b} = \frac{1}{\mathrm{n_c m_f Q_{LHV}}} \int_{\mathrm{t_{ign}}}^{\mathrm{t}} \frac{\mathrm{dQ_{net}+dQ_{HT}}}{d\theta} d\theta \tag{2.2}$$

As appears in the equations, several factors including the combustion efficiency, heat transfer and specific heat ratio and should be considered. Furthermore, to estimate the heat transfer, it is important to determine the end of combustion. It is well known that those factors varies depending on the operation condition, even the specific heat ratio varies as combustion progresses.

For the combustion efficiency, it is common to calculate using the enthalpy of exhaust gas, considering the gas composition. However, in this research, the

estimated heat release will be used for in-cylinder pressure prediction but it is impossible to measure the exhaust gas composition in real driving condition. Therefore, the combustion efficiency is assumed to be constant of 0.98.

The heat release rate is known to vary along in-cylinder temperature, so that it should be evaluated at each crank angle for better estimation. However, it leads to more calculation load and time which may make real time application difficult. In this research, the specific heat ratio was fixed to be 1.3 because it was considered not to be matter if same value is used for predicting in-cylinder pressure.

The amount of heat transfer was evaluated by subtracting net heat release from the heating value of supplied fuel. The supplied fuel mass was obtained from the flow meter and multiplied with the low heating value of fuel used. The amount of net heat release was calculated with accumulated heat release rate value at the end of combustion. Therefore, it was important to determine the end of combustion. Because the combustion phase varies diversely, fixing the end of combustion as specific timing is not proper assumption. In this research, Kim's method [36] was used. This method determines the end of combustion as 10 CA after when the multiplication of pressure and volume shows maximum value. It is shown in equation 2.3.

$$EOC = \theta_{\max(PV)} + 10 \text{ CA} \tag{2.3}$$

However, under the knocking condition, the pressure oscillation leads to faster determination of EOC. Therefore, low-pass filtered pressure was used for calculating the heat release rate. Kaiser windowing was selected as filtering method. In order to avoid signal phase shift from filtering, the zero-phase filtering method was used. The filter specification was selected to eliminate the pressure oscillation by knock while preserving other frequency component. Thus,

frequency analysis was carried out on the pressure signal with FFT. As a result, the passband frequency was 4 kHz and the stopband frequency was 5 kHz. The filter response magnitude plot are shown in figure 2.4.

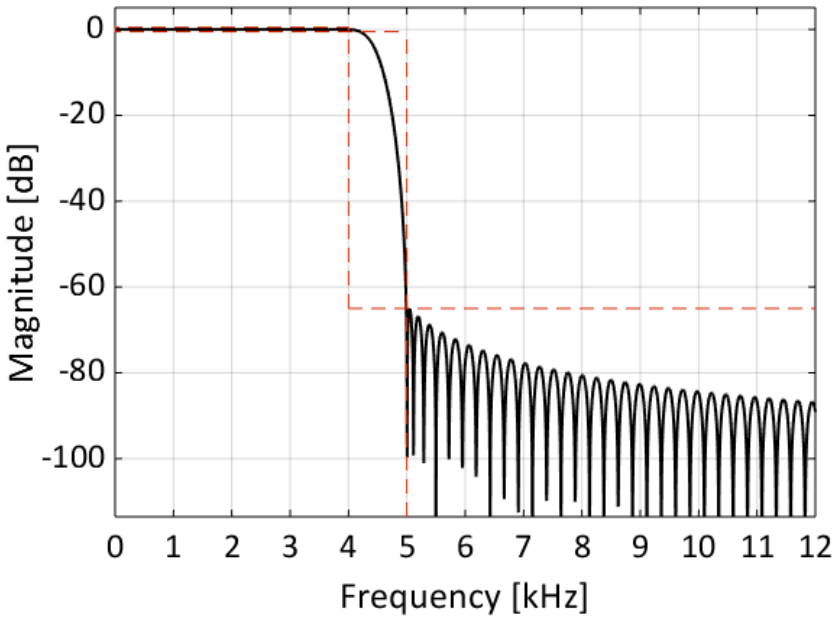

Figure 2.4 Magnitude response of filter

2.3.2 Knock onset determination

As many previous researches pointed out, MAPO-TVE method tended to determine knock onset later than it actually was. For Sharlari's method, it showed acceptable accuracy, but the accuracy deteriorated if the combustion phase was pushed back or knock was weak. It is thought because the algorithm detects stiff increase of pressure signal, which may appear by signal noise before knock occurs. Therefore, sometimes, it incorrectly estimated that knock occurred sooner than it actually did.

Therefore, in this research, the deep-learning method was introduced for knock onset determination. Normalized raw pressure data was used as model input and manually observed knock onset was back data for learning. Model was optimized by conducting parametric study on learning rate, number of hidden layer and epoch number. The model schematic and its specification are shown in figure 2.5. The developed model was validated with 1700 knocking cycles and showed less deviation of prediction depending on knock strength compared to existing methodologies.

. Figure 2.6 shows the comparison of each knock determination method. . The x-axis is actual knock onset of each cycle, which was manually picked by observing the start of pressure oscillation. The y-axis is determined knock onset by each method. As a result, it appears that the developed deep learning model determine knock onset precisely with less accuracy deviation.

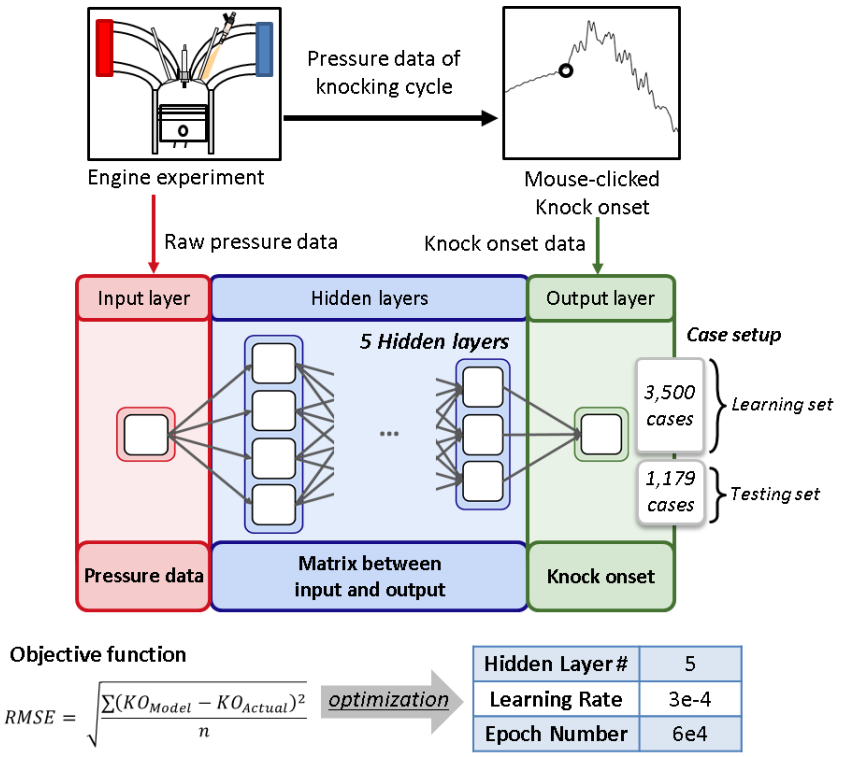

Figure 2.5 Schematic for deep learning model

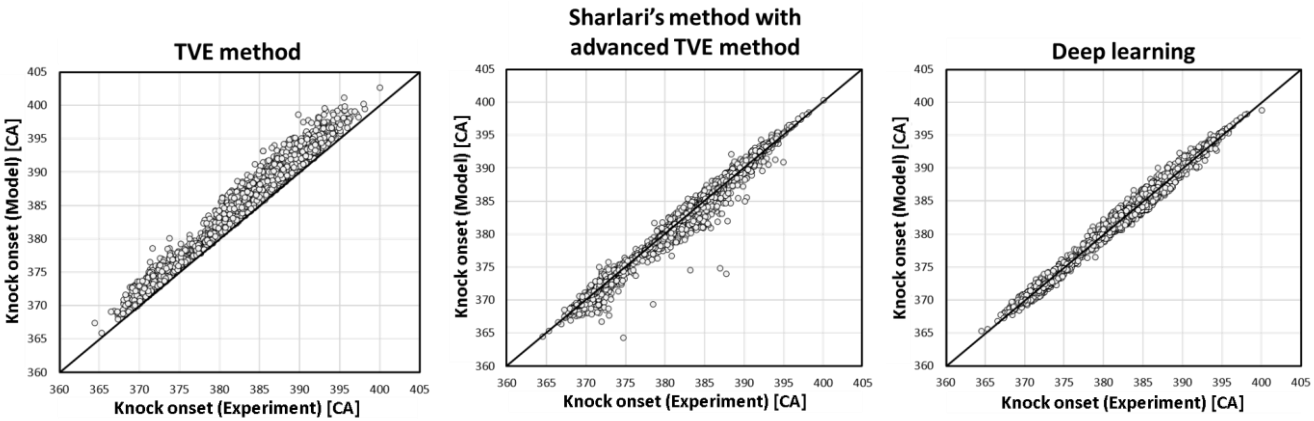

Figure 2.6 Comparison on methods for knock onset determination

2.3.3 Unburned gas temperature

Estimation of unburned gas temperature is essential for understanding ignition delay and auto-ignition. In this research, the unburned gas temperature was calculated with assumption of two zone model which regards the unburned gas region to be separated from burned gas region. To be precise, the heat transfer should be considered on temperature calculation because the unburned gas region is in contact with the combustion chamber wall. However, the auto-ignition occurs at hot spots inside unburned gas zone, not near boundary wall. Therefore, the temperature was estimated with assumption of adiabatic compression process. The equation is in equation 2.4. Though the specific heat ratio varies as temperature increases, its value was fixed as a constant of 1.3 for the same reason of the heat release calculation.

$$T_u = T_{IVC}\left(\frac{P_{cyl}}{P_{IVC}}\right)^{1-\frac{1}{\gamma}} \tag{2.4}$$

As appears in equation 2.4, the initial temperature of unburned gas is also important factor, however, it is hard to measure directly. Thus, it was calculated with the ideal gas equation as equation 2.5. Therefore, proper measurement of pressure at IVC, amount of trapped mass and its composition have considerable effect on temperature estimation.

$$P_{IVC}V_{IVC} = n_{total}RT_{IVC} \tag{2.5}$$

Due to the resolution limit of pressure transducer, the intrinsic error of 0.025bar appeared, which can cause 2 % ~ 5 % of error. So that, the smoothing methods were applied to pressure signal. For smoothing, the median filter with window of 9 points and 3rd order Savitzky-golay filter with 151 points were used.

Trapped mass consists of fuel, air and residual gas. For the fuel, the monitored value with the flow meter was used. Air mass was calculated by multiplying stoichiometric air-fuel mass ratio to fuel mass because the engine was operated under stoichiometric condition. However, in case of the residual gas, it should be modelled because it is difficult to measure or estimate by pressure data.

2.3.4 Residual gas fraction estimation

The residual gas fraction (RGF) is important factor, not only for the trapped mass, but also for the gas composition, which affects the gas constant and specific heat ratio. However, the direct measurement of RGF is very difficult because it is a kind of internal EGR. Though several researches about measurement of RGF exist, they require measurement of other indirect sources such as CO2, THC and NOx [52, 53, 54, 55].

Numerous modeling approaches also have been conducted to estimate the residual gas fraction. As initiative, Fox et al.[56] assumed that the residual gas was trapped by burned gas in the clearance volume and backflow of exhaust gas. With the assumption of the ideal Otto cycle, they introduced the RGF model. This model considers the manifold pressure, compression ratio, engine speed and valve overlap. To quantify the valve overlap, they introduced the overlap factor, which means the average valve curtain area during valve overlap. The equation for overlap factor is shown in equation 2.6. D is valve diameter and L is valve lift.

$$OF = \frac{D_{In}\int_{\theta_{IVO}}^{L_{In}=L_{Ex}} L_{In}d\theta + D_{Ex}\int_{L_{In}=L_{Ex}}^{\theta_{EVC}} L_{Ex}d\theta}{V_d} \tag{2.6}$$

After Fox, many researchers have tried to modify his 0-D model for better accuracy and universality. [57, 58, 59]. Recently, Kale et al. [60] developed a RGF

model which distinguishes the valve overlap duration with consideration on the location of TDC and timing with same intake/exhaust valve curtain area. Although this model has 13 of tuning coefficients, it shows relatively accurate result.

However, due to the empirical and simplified form of the model, it occasionally gave negative value of RGF under conditions with high volumetric efficiency. Therefore, adjustment was conducted by changing the effect of the volumetric efficiency from linear to an exponential. The model is as followed.

$$RGF = RGF_{IVC} + RGF_{Backflow} \tag{2.7}$$

$$RGF_{IVC} = \frac{e^{C_1 VO} OF_{s.IVC} OF_{ns.IVC}}{Speed * CR_{eff}} \left(\frac{P_{Ex}}{P_{In}}\right)^{\frac{1}{\gamma}} \tag{2.8}$$

$$OF_{s.IVC} = C_2 OF_{C.In} + C_3 OF_{C.Ex} + {\eta_v}^{C_4} + C_5 \tag{2.9}$$

$$OF_{ns.IVC} = C_6 (OF_{C.In} - OF_{C.Ex}) + {\eta_v}^{C_7} \tag{2.10}$$

$$RGF_{Backflow} = \frac{e^{C_8 Speed} OF_{s.back} OF_{ns.back}}{Speed} \left(\frac{P_{Ex}}{P_{In}}\right)^{\frac{\gamma+1}{2\gamma}} \sqrt{|P_{Ex} - P_{In}|} \tag{2.11}$$

$$OF_{s.Back} = C_9 (OF_{TDC.In} + OF_{TDC.Ex}) + C_{10} (OF_{C.In} + OF_{C.Ex}) + \frac{C_{11} \eta_v}{\lambda} \tag{2.12}$$

$$OF_{ns.Back} = C_{12} (OF_{TDC.In} - OF_{TDC.Ex}) + C_{13} (OF_{C.In} - OF_{C.Ex}) \tag{2.13}$$

$$OF_{C.In} = \frac{D_{In} \int_{\theta_{IVO}}^{Area_{In} = Area_{Ex}} L_{In} d\theta}{V_d} \tag{2.14}$$

$$OF_{C.Ex} = \frac{D_{Ex} \int_{Area_{In} = Area_{Ex}}^{\theta_{EVC}} L_{Ex} d\theta}{V_d} \tag{2.15}$$

$$OF_{TDC.In} = \frac{D_{In} \int_{\theta_{IVO}}^{TDC} L_{In} d\theta}{V_d} \tag{2.16}$$

$$OF_{TDC.Ex} = \frac{D_{Ex} \int_{Tdc}^{\theta_{EVC}} L_{Ex} d\theta}{V_d} \tag{2.17}$$

In order to calibrate the tuning constants, real RGF value was necessary. However, as mentioned, measuring reliable RGF data is challenging task. Therefore, instead of measurement, a 1-D simulation model was built with GT-power software. The model geometry was modified to produce the same in-cylinder and intake manifold pressure trace under the motoring condition. The matched motoring pressure is depicted in figure 2.7 and combustion pressure in figure 2.8.

After that, the implanted combustion model, SITurb model, was calibrated to match the combustion pressure trace with that from experiment. With the calibrated model, various operation points were simulated to obtain RGF value under each condition. The calibrated model constants and simulated conditions are shown in table 2.3 and 2.4.

Then, the modified 0-D RGF model was calibrated with the back data from GT-power. The exhaust manifold pressure was fixed at 1.013bar since it cannot be measured in the environment in which this model will be implanted. For optimization, the genetic algorithm was used due to many tuning constants. Figure 2.9 shows the comparison between existing models and the modified model. All of models were calibrated to same back data from GT-power.

With developed model, the mass of residual gas was calculated as in equation 2.18 and the total number of mole was calculated as in equation 2.19.

$$m_r = \frac{x_r m_f (1+AFR)}{1-x_r} \tag{2.18}$$

$$n_{total} = \frac{m_f}{M_f} + \frac{m_a}{M_a} + \frac{m_r}{M_r} \tag{2.19}$$

To estimate the molar mass of fuel, its composition was assumed to be PRF, with 91.5 % iso-octane and 8.5 % normal-heptane, regarding the octane number of fuel. For air, it was assumed to be 21 % oxygen and 79 % nitrogen. In case of

the residual gas, a simple chemical reaction was considered with assumption of complete combustion. In this equation, the real H/C ratio of test fuel was used for the reliable estimation of the composition of reaction product gas. The reaction is as followed in the equation 2.20.

$$C_1H_{2.064} + 1.516(O_2 + 3.773N_2) \rightarrow 1.032H_2O + CO_2 + 5.720N_2 \quad (2.20)$$

With determined gas composition, the molar mass of each gas was calculated as followed in the equation 2.21.

$$M_i = \sum_j x_j M_j$$

$$(i : fuel, air, residual\ gas,\ j : arbitrary\ species\ in\ gas) \quad (2.21)$$

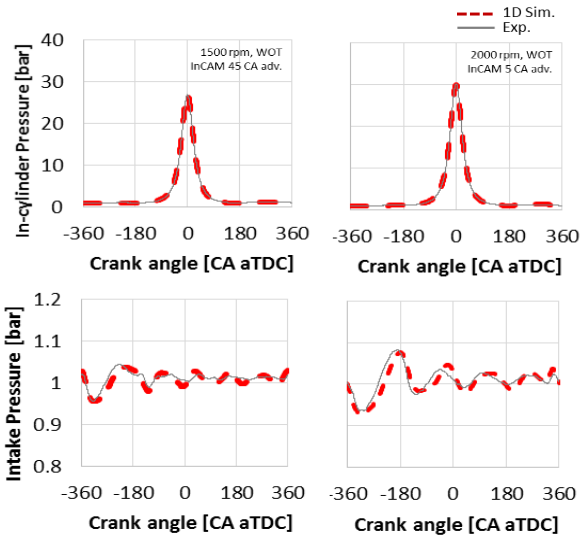

Figure 2.7 Motoring condition matching with GT-power

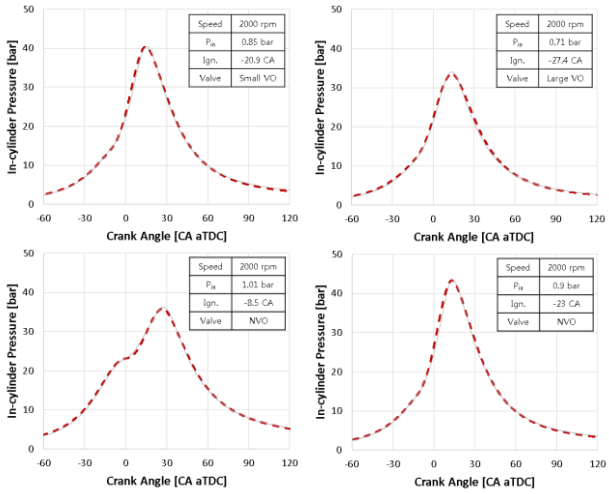

Figure 2.8 Combustion matching with GT-power

Table 2.4 SITurb model calibration

Parameter (SITurb / Woschni)	**Optimized value**
Flame Kernal Growth Multiplier	1.167
Turbulent Flame Speed Multiplier	0.690
Taylor Length Scale Multiplier	0.703
Woschni Multiplier	0.7

Table 2.5 Simulation condition

Sweep parameter	**Range**
Engine Speed [RPM]	1500 - 3000
Ignition Timing [CA bTDC]	28 – 0
Intake pressure [bar]	0.2 – 0.9
InCAM adv. [CA]	0 – 40
ExCAM rtd. [CA]	0 – 3
Total 1200 cases	

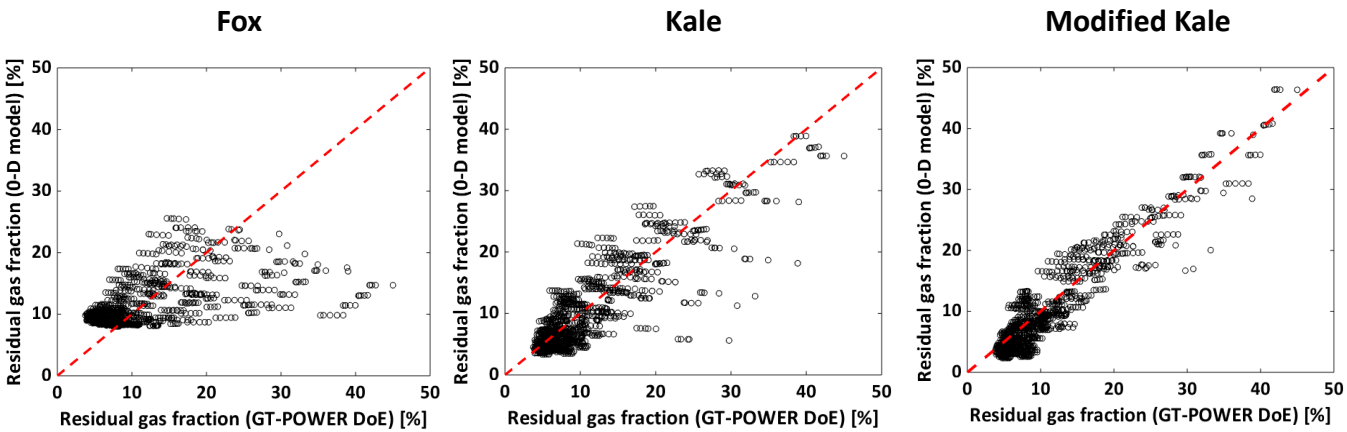

Figure 2.9 Comparison of RGF models; Fox (left), Kale (center) Modified Kale (right)

Chapter 3. Model Description

3.1 Prediction of in-cylinder pressure

3.1.1 Initial gas state

3.1.1.1 In-cylinder pressure at IVC

Incorrect estimation of initial gas state can result in critical error on overall procedure of knock prediction. Especially, in-cylinder pressure at IVC has significant effect because it affects all the factors related to ignition delay, including pressure, density and temperature. Though the mass-production engines are equipped with the manifold air pressure (MAP) sensor, it is known that the in-cylinder pressure is not equal to the manifold pressure due to temperature and gas flow. Therefore, it is necessary to investigate the correlation between the manifold pressure and the in-cylinder pressure at IVC.

Eriksson et al. [61] introduced a correlation considering the engine speed. However, that correlation was not valid when applied to measured data with different valve timing. Therefore, the effect of valve timing was considered in terms of the overlap factor, which was introduced by Fox et al. [56]. The modified correlation is expressed in equation 3.1 and the comparison is depicted in the figure 3.2.

$$P_{Cyl,IVC} = P_{Mani,IVC} + 0.078 - 0.024Speed - 0.0016\mathrm{OF} \quad (3.1)$$

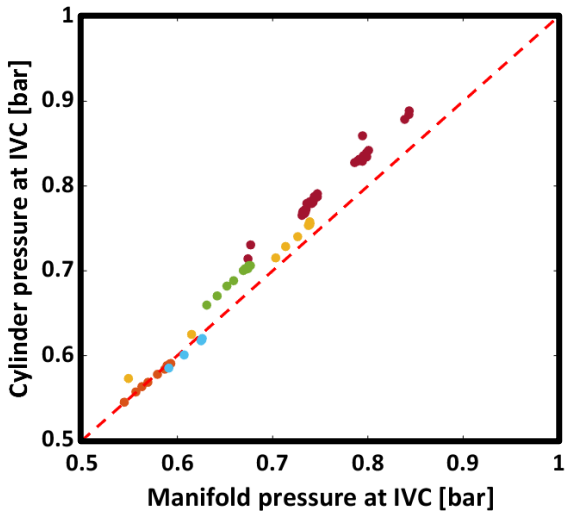

Figure 3.1 Manifold pressure vs. In-cylinder pressure at IVC

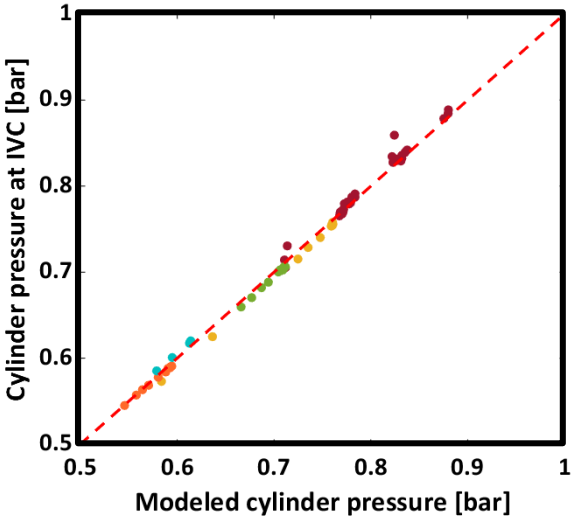

Figure 3.2 Estimated in-cylinder pressure at IVC

3.1.1.2 Initial gas temperature

As mentioned in in Chapter 2.3.3 and Chapter 2.3.4, the initial gas temperature was estimated with the ideal gas equation. The in-cylinder pressure at IVC was predicted with the correlation in equation 3.1 and EMS data including MAP sensor data, engine speed and valve configuration. Trapped mass was estimated based on the fuel injection rate, air-fuel ratio and the residual gas fraction model. The molar mass of each gas mixture was stored in the form of array and used to calculate the number of moles.

3.1.2 Compression process with polytropic index model

When analyzing the dynamics of a heat engine, the compression process is generally assumed as the polytropic process as equation 3.2.

$$P_1 \mathrm{V}_1{}^{k} = P_2 \mathrm{V}_2{}^{k} \tag{3.2}$$

If the polytropic index, k, can be determined as a specific constant, the estimation of compression process would become much simpler. However, it is known that the polytropic has a value of about 1.3 ±0.5 [7], which varies depending on operating condition. Furthermore, incorrect determination of the polytropic index leads to wrong estimation of in-cylinder pressure at the spark timing as shown in figure 3.3. Because the in-cylinder pressure at the spark timing is initial condition for predicting the pressure during combustion, it is important to estimate the polytropic index properly.

Lee et al. [62] introduced a polytropic index estimation model for CI engines. They found that the polytropic index varies almost linearly along the amount of heat transfer during compression divided by initial temperature. Therefore, the

model has the form of linear equation. The equation is briefly shown in equation 3.3.

$$k = k_{isen} + \frac{Q_{HT}}{T_{IVC}} * Slope \quad (3.3)$$

The y intercept of equation meant representative γ during compression, noted as k_{isen}. Because the change of k_{isen} majorly depends on the temperature and gas composition, k_{isen} was modelled as combination of T_{IVC}, γ_{IVC} and $CR_{IVC\text{-}SOI}$ (volume ratio between IVC and SOI). Slope was modelled as form of inversely proportional to $CR_{IVC\text{-}SOI}$ by conducting sensitivity analysis. For heat transfer, woschini's correlation was used with calibration for the test engine.

Lee's model consists of the key factors that have major influence on the polytropic index with their physical meaning. However, considering the model in the view of only the form of formula, the model can be regressed as multiplication of P, T, γ and $CR_{IVC\text{-}SOI}$. Therefore, in this research, the model was regressed as in equation 3.4.

$$k = C_1 {\gamma_{IVC}}^{c_2} {CR_{IVC-ign}}^{c_3} Speed^{C_4} \quad (3.3)$$

γ_{IVC} was calculated using T_{IVC} and the curve-fit coefficients table for specific heat [Turns]. In order to calibrate the coefficients, polytropic index for each condition was calculated with measured pressure data as shown in equation 3.4. The RMSE between k and k_{exp} was selected as the objective function of model optimization. The calibration result is depicted in figure 3.4 and comparison between measure pressure and predicted pressure at spark timing is shown in figure 3.5.

$$k_{exp} = \log(P_{ign}/P_{IVC}) / \log(V_{IVC}/V_{ign}) \quad (3.4)$$

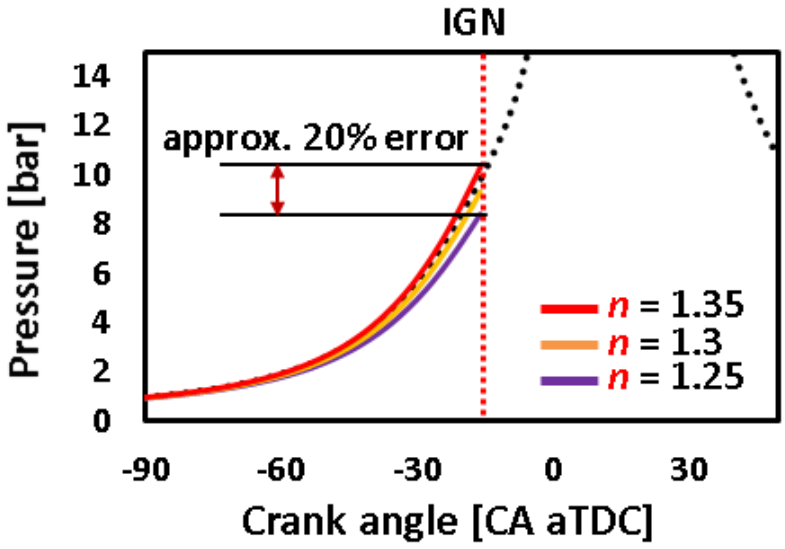

Figure 3.3 Incorrect estimation of pressure at IGN.

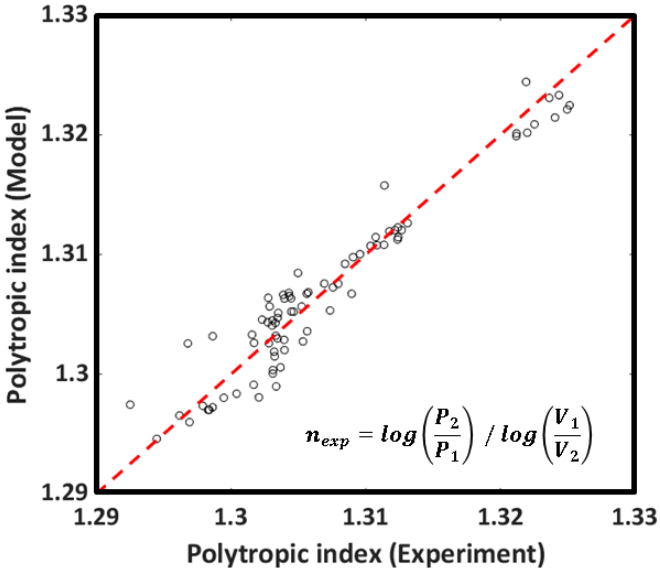

Figure 3.4 Estimation of polytropic index

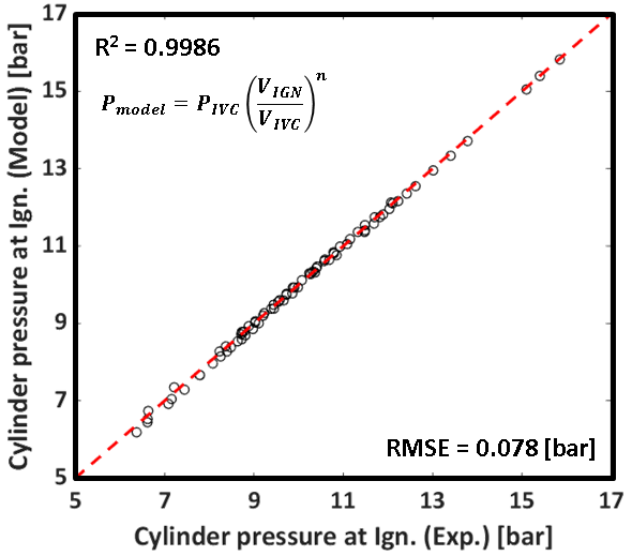

Figure 3.5 Estimation of in-cylinder pressure at spark timing

3.1.3 Combustion process estimation

3.1.3.1 Accumulated heat release and in-cylinder pressure

In Chapter 2.3.1, it is mentioned that the net heat release rate can be calculated with the measure in-cylinder pressure. Therefore, in opposite way, it is possible to calculate the in-cylinder pressure with the net heat release rate. The equation 3.5 shows the recurrence relation of in-cylinder pressure, derived by simple arithmetic calculation.

$$P_n = \frac{\frac{dQ_{net}}{d\theta} - \frac{\gamma}{\gamma-1}P_{n-1}\frac{dV}{d\theta}}{\frac{1}{\gamma-1}V_{n-1}\frac{1}{d\theta}} + P_{n-1} \tag{3.5}$$

As shown in equation 3.5, it is essential to accurately predict the net heat release rate in order to estimate the pressure trace. However, because the operating range of the engine is much wide, it is difficult to make reliable prediction of the net heat release rate for all operating conditions.

3.1.3.2 Wiebe function and a representative heat release curve

Wiebe function is traditionally known to match the burn rate curve well with appropriate calibration. The formula is expressed in equation 3.6.

$$x_b = 1 - \exp(-a\left(\frac{\theta-\theta_{ign}}{\theta_b}\right)^{m+1}) \tag{3.6}$$

Furthermore, when the accumulated net heat release rate is expressed in terms of the mass fraction burned, it can be written as equation 3.7.

$$Q_{net}(\theta) = (Q_{fuel} - Q_{loss})(1 - \exp\left[-a\left(\frac{\theta-\theta_{ign}}{\theta_b}\right)^{m+1}\right]) \quad (3.7)$$

Therefore, the parameters a, m, θ_{ign}, θ_b and Q_{loss} should be determined to estimate the net heat release rate and in-cylinder pressure. Of these parameter, θ_{ign} can be specified as the spark timing, but the rest are difficult to be determine because they vary greatly depending on the operation condition.

Lee [63] assumed that a representative "a" and "m" value of an engine can be found with the normalized burn rate curve. The burn rate curves from experiment were normalized by burn duration and accumulated net heat release. Those curves were collected and used for determining the "a" and "m" value by calibrating the normalized Wiebe function in equation 3.8.

$$Q_{norm}(\theta) = 1 - \exp[-a(\theta)^{m+1}] \quad (3.8)$$

In this research, Lee's concept was implemented for the heat release rate prediction. For the normalization, accumulative net heat release was calculated with measure pressure and specific heat ratio of 1.3. These AHRR curves were normalized; for the x axis, the spark timing to CA90 was used, and for the y axis, Q_{net} value at EOC was used. Figure 3.6 demonstrates the characterization of heat release curve.

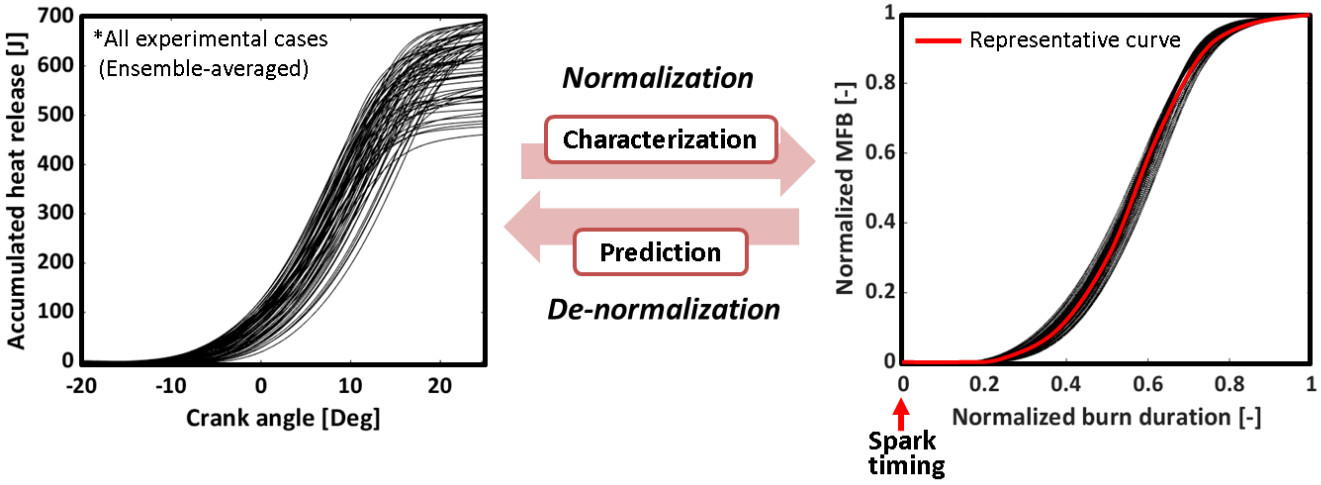

Figure 3.6 Characterization of heat release

3.1.3.3 Burn duration and heat loss models

The θ_b and Q_{loss} are also needed to be determined under each condition to complete the heat release rate prediction. Those parameters have been continuously analyzed, and as a result, it is well known which physical properties have major effect on them. Therefore, the burn duration and heat loss were predicted with proper 0-D models.

For the burn duration, Bonatesta's 0-D model [64] was applied with calibration. This model considers the effect of load, dilution, turbulence and combustion phase in terms of gas density at spark timing, EGR, piston speed and the spark timing respectively. For this research, the EGR term was excluded because the EGR gas was not supplied in experiment. As a result, the model was constructed as the formula in equation 3.9.

$$\theta_b = 1466.3{\rho_{ign}}^{-0.35}\left(1-\frac{1.02}{\sqrt{V_p}}\right)\left(7.4*10^{-4}{\theta_{ign}}^2-0.036\theta_{ign}+1\right) \quad (3.9)$$

The gas density was calculated with estimated trapped mass and volume at spark timing. For mean piston speed, it was determined with the stroke and engine speed. θ_{ign} means the spark timing in bTDC crank angle. The model was calibrated to match the duration from the spark timing to CA90, which was calculated from measured pressure data. The calibration result is depicted in figure 3.7.

For the heat loss, using conventional heat transfer model can be considered, such as Woschini, Hohenberg and other 0-D models for heat transfer coefficient. However, these heat transfer models require to be updated at each crank angle as the gas state varies, which leads to more calculation and complexity. Therefore, a simple 0-D model, considering engine load, combustion phase and engine speed, was introduced. The higher engine load and faster combustion phase leads to more

heat transfer due to more temperature rise. The engine speed was considered for gas flow speed and heat transfer time. The developed model is shown in equation 3.10.

$$Q_{loss} = 68.45(\mathrm{m_{fuel}})^{1.34}(\mathrm{Speed})^{-0.43}\left(\theta_{\mathrm{ign}}\right)^{-7.27} \quad (3.10)$$

The back data for heat loss model calibration was prepared by subtracting the net released heat at EOC from the product of fuel mass and low heating value. The figure 3.8 shows the calibration result of heat loss model.

Finally, these two models and the Wiebe parameters; "a", "m" were inserted to equation 3.7. After that, with the equation 3.5 and equation 3.7, the in-cylinder pressure was predicted. The prediction result is shown in figure 3.9.

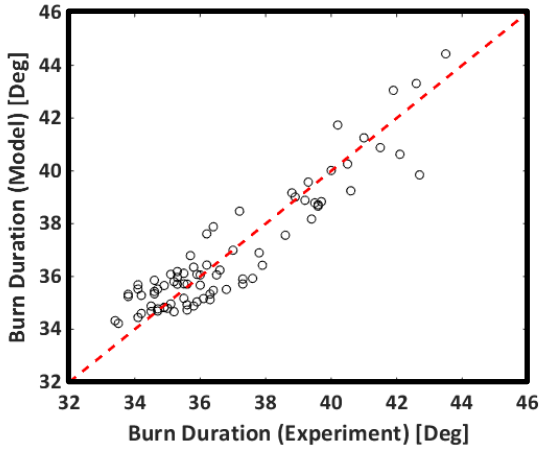

Figure 3.7 Model calibration for burn duration,

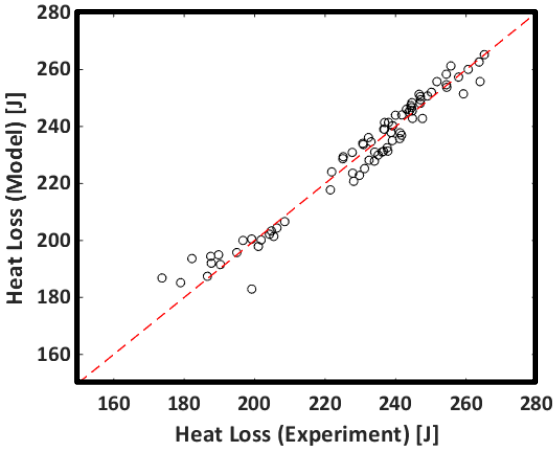

Figure 3.8 Model calibration for heat loss

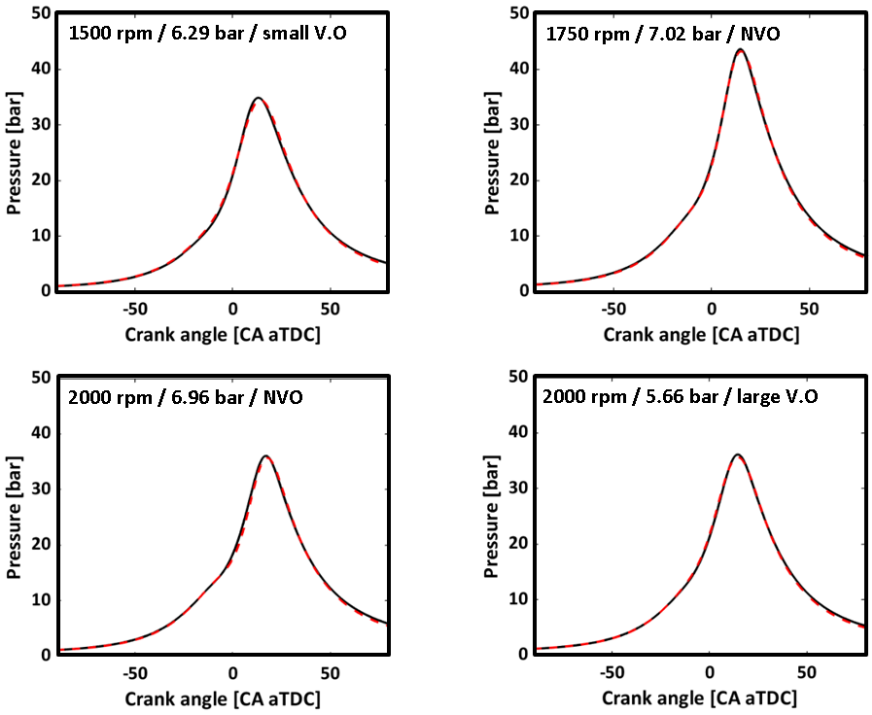

Figure 3.9 Predicted in-cylinder pressure

3.1.4 Simulation of cyclic variation

Estimation of cyclic variation is also important because the condition of individual cycle determines knock occurrence, not the mean operating condition. However, the cyclic variation is involved with numerous factors, some of which shows even random characteristics. Thus, it is difficult to simulate the cyclic variation exactly.

Cho et al. [51] used a simple method to simulate cyclic variation with consideration on the variation of Wiebe function parameters. The accumulated heat release rate curve of each cycle was fitted to the Wiebe function and the distributions of the coefficients; “a”, “m” and burn duration were obtained. This methodology was applied to this research.'

However, in this research, distribution of only “a” and “m” was considered because the burn duration was modeled with mean operating condition. Therefore, when conducting the curve fitting, the burn duration of cycles in same experiment condition was fixed as averaged burn duration. The obtained distribution of two parameters are shown in figure 3.10 and 3.11. These probability distributions were divided into 10 sections each and combined into 10 by 10 probability map for combination of “a” and “m”. The probability map is shown in figure 3.12. The resulted 100 of combinations of “a” and “m” were used to simulate the pressure trace with cyclic variation at each condition.

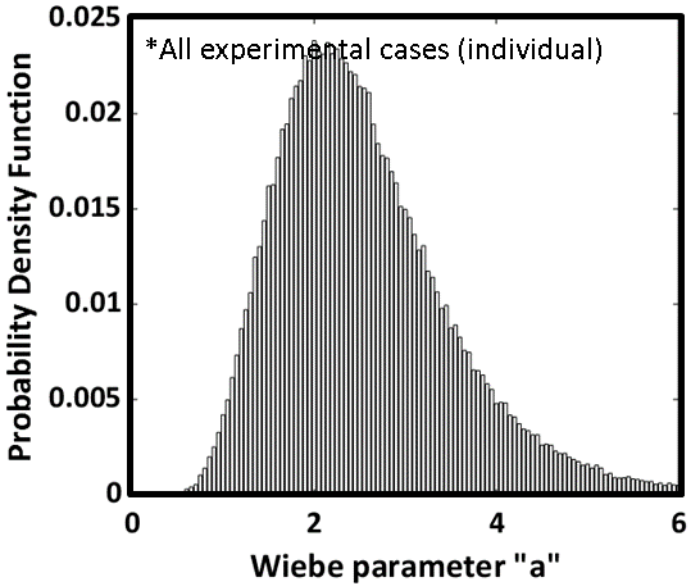

Figure 3.10 Probability distribution of the Wiebe parameter "a"

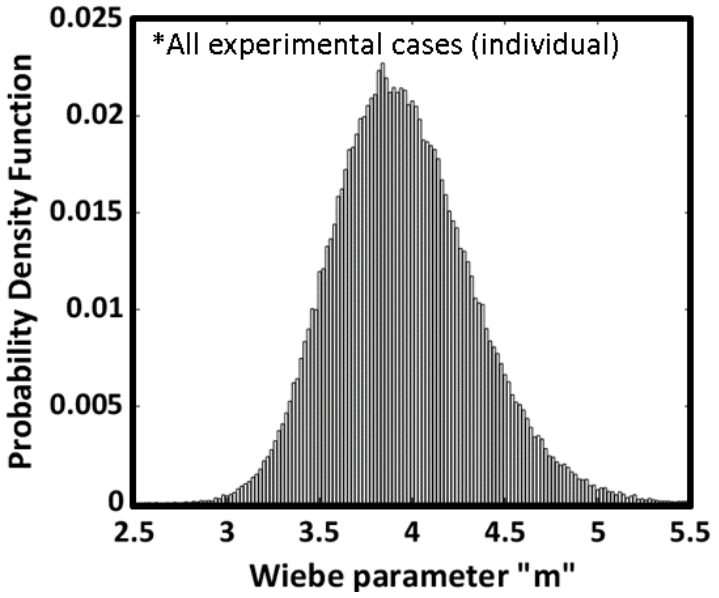

Figure 3.11 Probability distribution of the Wiebe parameter "m"

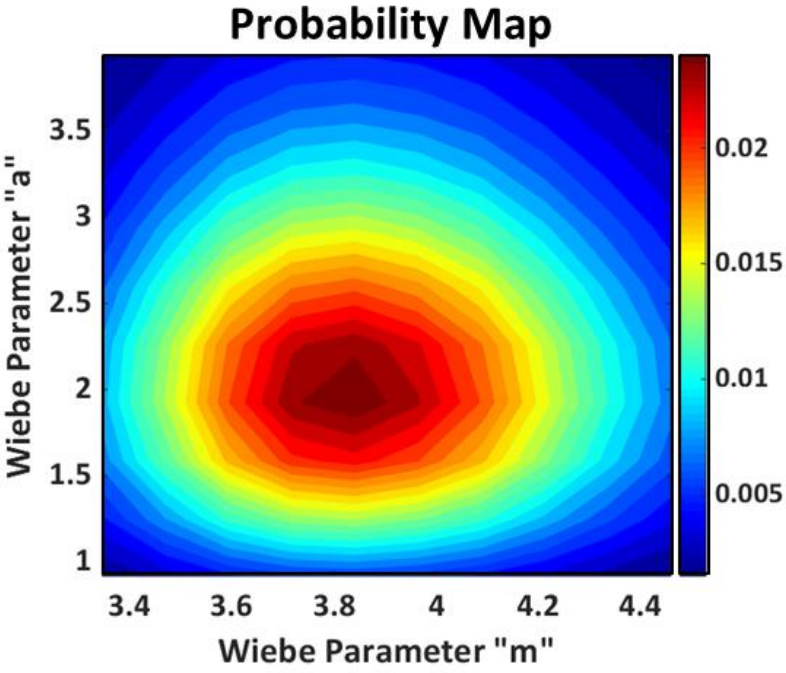

Figure 3.12 Probability map for combinations of the Wiebe parameters

3.2 Criteria for knock determination

3.2.1 Ignition delay estimation

Because the auto-ignition is known as the necessary condition for knock, the ignition delay should be estimated to determine the possibility of knock occurrence. As mentioned in Chapter 1.2.1, there are models that consider various factors affecting combustion such as EGR, equivalent ratio and octane number. However, since those factors were net considered in this research, simplified Cho's model in equation 3.11 was used with calibration.

$$\tau = 6.91 * 10^{-6} \left(\frac{P}{T}\right)^{-1.9} exp\left(\frac{5413}{T}\right) \tag{3.11}$$

Actual knock onset was obtained by developed deep learning model with measure pressure trace. For the optimization method, the genetic algorithm was used because the order of coefficients was so different that the general optimization methods tended to be induced to local optimal point. The calibration result is shown in figure 3.13. The detailed specifications of optimization parameters are informed in the table 3.1.

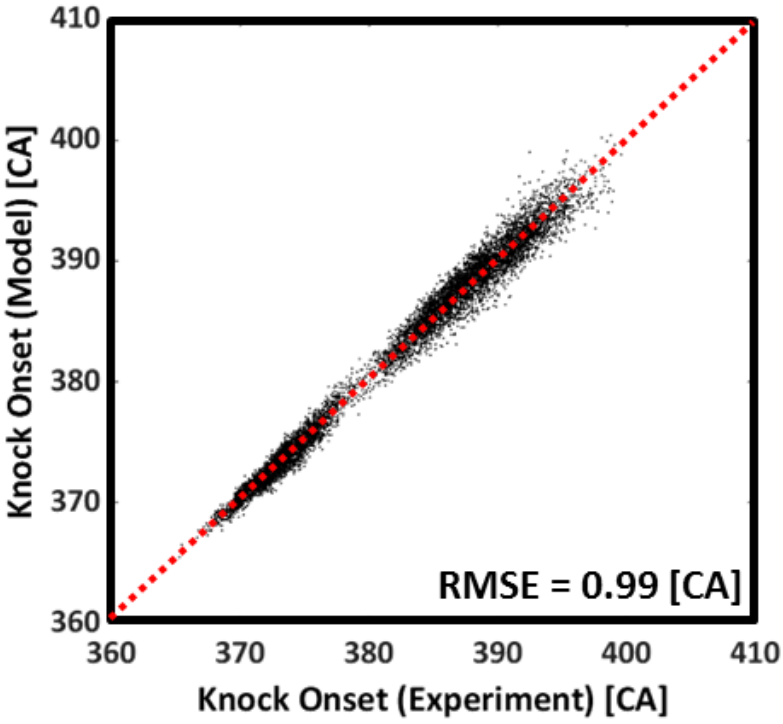

Figure 3.13 Calibration result for ignition delay model

Table 3.1 Parameters for the genetic algorithm

Optimization Method	Genetic Algorithm
Population	1,000
Crossover	0.7
Mutation	0.3
Tolerance	1e-4
Generation limit	25
Objective function	RMSE

3.2.2 Mass burned fraction and knock onset

In general circumstances, it is thought that auto-ignition would occur when the ignition delay is over. However, in case of knock determination, there may occur a situation that no remaining unburned gas exists at the end of ignition delay. In other words, the ignition delay only informs when the auto-ignition would occur, but does not gives whether it occurs or not. Furthermore, Livengood-Wu integral keeps accumulating the inverse of ignition delay regardless of existence of unburned gas. Therefore, the integral value often reaches unity even under low load condition as in figure 3.14. So, the additional criterion is required for knock determination.

Since knock can occur only if the unburned gas exists, it was thought that the MFB value at knock onset could be the additional criterion. In figure 3.14, it can be found that the predicted knock onset timing was advanced faster than the MFB 85 timing was as knock incidence increased. Even under low knock incidence condition, the predicted knock onset became later than the MFB85 timing.

Thus, it was decided that the knock occurred if the MFB value at the predicted knock onset was below a certain value, and vice versa. In order to determine proper threshold value, the distribution of MFB value at knock onset was identified as demonstrated in figure 3.15. It was found that the probability of knock occurrence decreased stiffly after MFB80 timing and the probability was even less than 5 % after MFB 85. Therefore, both MFB80 and MFB85 were tested for determine threshold value. The result will be present in the next chapter.

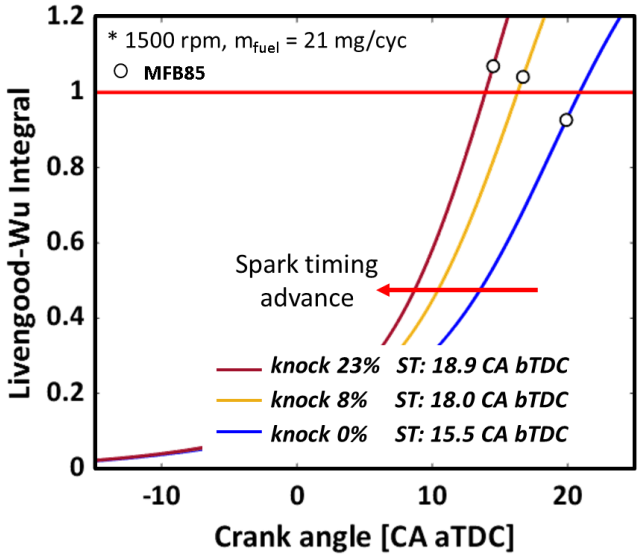

Figure 3.14 Livengood-Wu integral and knock incidence

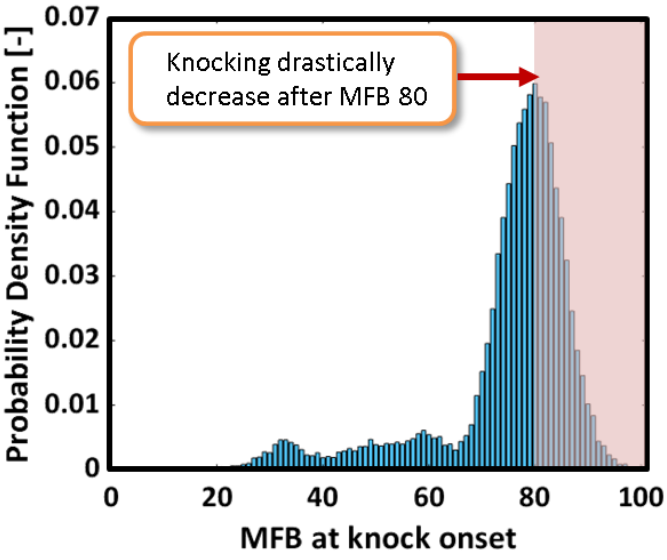

Figure 3.15 Knock onset and MFB

Chapter 4. Result and discussion

The obtained EMS data at each experiment condition were put into the developed model as input values. By using the predicted in-cylinder pressure and ignition delay model, the MFB and knock onset were also predicted. As mentioned in the chapter 3.2.2, the correlation between predicted knock onset and MFB80/85 was scattered in figure 4.1. The blue dots represent the experiment cases with normal operating condition, with knock incidence less than 3 %. The red dots mean the knock-prone condition, with knock incidence more than 25 %. It was found that both MFB80 and MFB85 seemed to be appropriate threshold for distinguishing knock-prone and non-knocking condition, but MFB85 appeared to be a bit better for conservative knock avoidance control.

To validate the model with the threshold of MFB85, the prediction of the in-cylinder pressure with cyclic variation was conducted for each operating condition using the method in Chapter 3.1.4. With each pressure trace, the knock onset and MFB85 timing were calculated and compared to determine knock occurrence. The examples are shown in figure 4.2. The red colored combination means the knock-prone condition and the blue colored is non-knocking combination.

Figure 4.3 describes the method to estimate knock incidence with the probability map of each parameter combination. A value of 1 was given for the red region (knock-prone region) and 0 was given for the blue region (non-knocking region). This binary knock occurrence map was multiplied with the probability map of the Wiebe parameters as equation 4.1. f is probability of combination with i th "a" value and j th "m" value. δ(i,j) is 0 or 1 regarding the knock occurrence with i th "a" value and j th "m" value.

$$Knock\ Incidence = \sum_i \sum_j f(i,j)\delta(i,j) \tag{4.1}$$

In this way, the knock incidence under each operating condition was estimated. As shown in figure 4.3, the prediction results were highly correlated with actual knock incidence and can be concluded to be accurate. The accuracy was deteriorated under weak knock condition with knock incidence less than 20 %. However, because the weak knock is not critical to engine durability, this failure of prediction was thought to be acceptable.

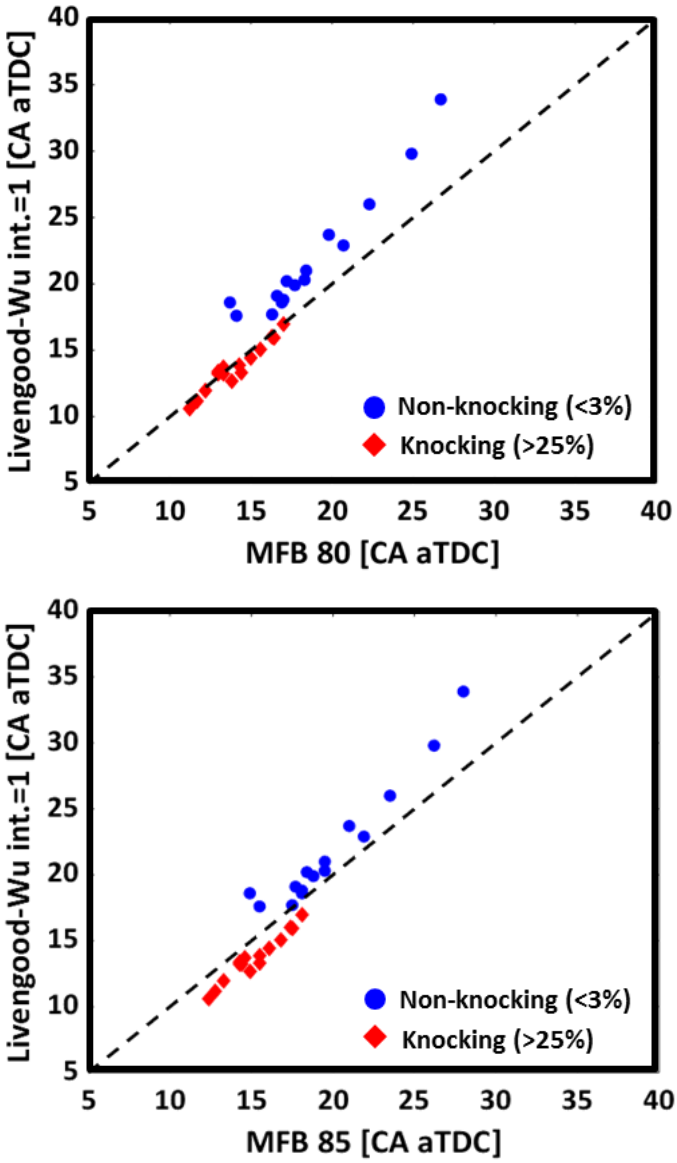

Figure 4.1 Knock determination with MFB

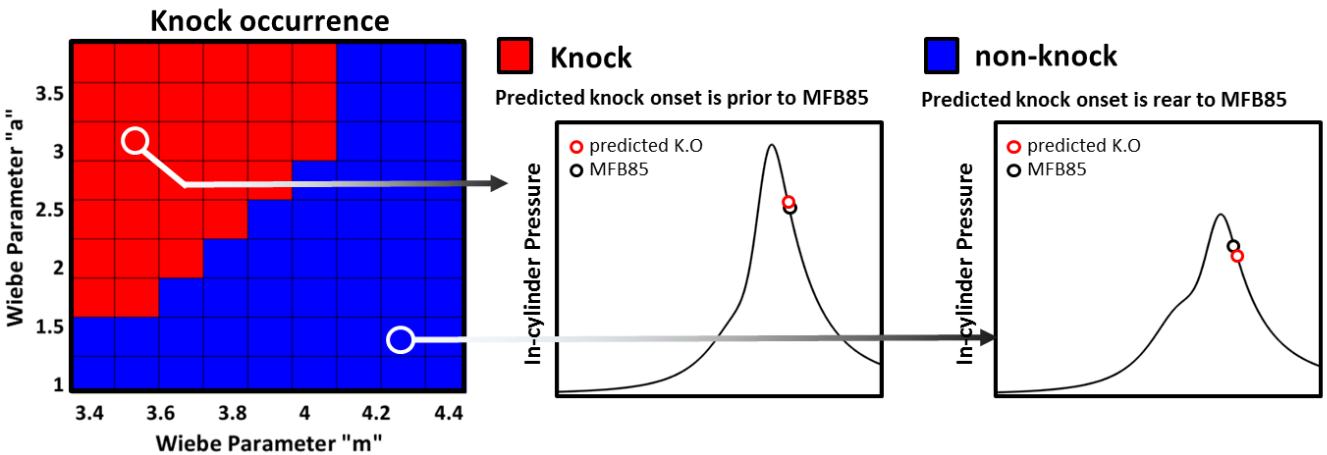

Figure 4.2 Knock prediction with cyclic variation

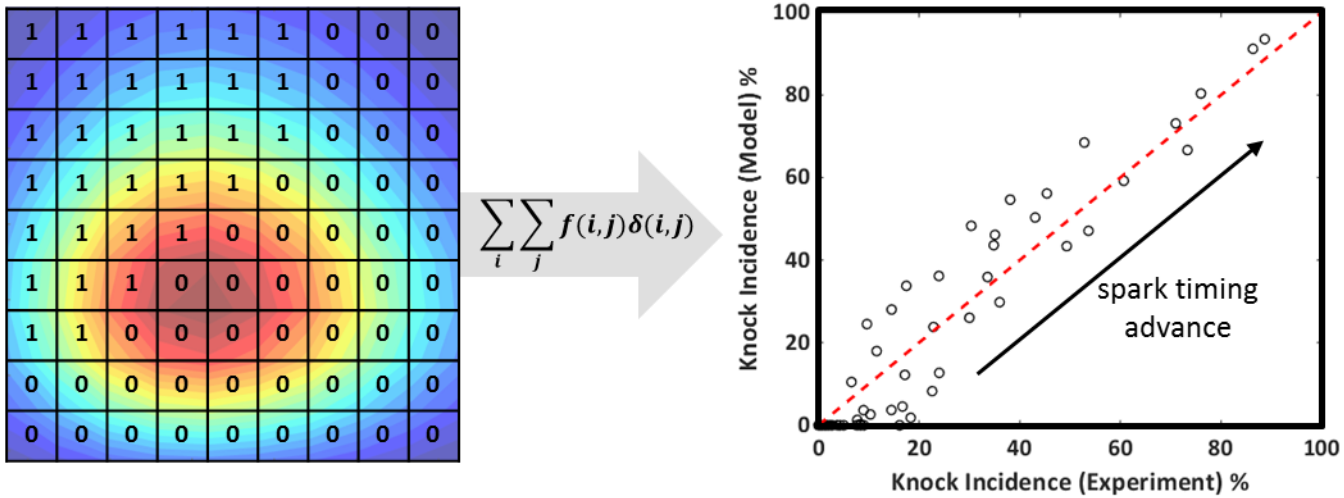

Figure 4.3 Knock incidence prediction

Chapter 5. Conclusion

In this research, a knock prediction model for a spark-ignited engine was developed. For the application to mass-production engines, the developed model takes the inputs such as available sensor signal or operating parameters from only EMS. Furthermore, considering the application to real-time control of operating parameters, the fast prediction was required. Therefore, the models was constructed in zero-dimension.

As the knock phenomena is quite sensitive to specific engine and operating condition, the precise prediction of in-cylinder pressure under various operating condition was essential. Therefore, the engine test was conducted to obtain back data for developing the pressure prediction model. The used engine was a single cylinder SI engine with CVVT module. For operating variables, the fuel rate, spark timing and valve timing was selected. The acquired pressure trace was used to calculate the combustion characteristics such as heat release rate, burn duration and heat loss.

Pressure prediction model consisted of three steps; initial gas state at IVC, compression process and combustion process. For the initial gas state, the correlation between the intake manifold and in-cylinder pressure was established with engine speed and valve phase. In order to calculate the initial temperature, trapped mass at IVC was estimated with air, fuel and residual gas. The air mass was calculated with air-fuel ratio and fuel injection rate.

For the residual gas fraction, existing 0-D model was modified and calibrated. Back data for calibration was obtained from a 1-D simulation model by GT-power software. The geometry of model was adjusted to precisely simulate the gas flow in the manifold and cylinder. The implanted combustion model was calibrated to

match measured pressure. Following this procedure, the RGF values for 1200 different conditions were obtained.

The compression was assumed to be the polytropic compression process. Thus, the polytropic index during compression was estimated considering specific heat ratio, compression ratio and engine speed. The specific ratio was calculated with the initial temperature and coefficient table for polynomial for specific heat.

The combustion pressure prediction, the concept of representative heat release curve was applied. The calculated heat release from experiment was normalized by burn duration and net heat release. The obtained curves were fitted to one normalized Wiebe function. In order to conduct de-normalization of the representative curve to actual heat release rate, modelling on the burn duration and heat loss was also carried out. As a result, by inversing the heat release rate to combustion pressure, the in-cylinder pressure was estimated accurately under various conditions.

The cyclic variation was simulated with the variation of the Wiebe function parameters. Distribution of each parameter was analyzed in terms of probability density function. By combining those probability, the representative probability table was generated for an engine.

Estimation of ignition delay was essential for predicting knock occurrence. Therefore, a 0-D ignition delay model was calibrated with experiment result. Measured pressure and calculated unburned gas temperature was used for model calculation. For calibration, actual knock onset was collected by using a knock onset determination model. Because the ignition delay model consists of exponential terms and the coefficients have various order, the genetic algorithm was applied to optimization.

However, the ignition delay only gives the onset of auto-ignition, not the occurrence of auto-ignition. Thus, the mass fraction burned was used as an additional criterion for knock determination, considering the maintained mass of unburned mixture.

With both models and criterion, the possibility of knock at each condition was estimated and it was possible to distinguish the knock-prone condition from normal operating condition. Furthermore, the model was validated with the simulation for cyclic variation. The model prediction result showed accurate result on estimating knock incidence, which was judged that the developed model showed reliable result at various condition. Therefore, the developed model is thought to be applicable for actual engine operation after additional calibration to each engine.

Bibliography

[1] Tietge, U. Co2 emissions from new passenger cars in the eu: Car manufacturers' performance in 2017. ICCT, 2018.

[2] Heywood, J. B. and MacKenzie, D. On the road toward 2050: Potential for substantial reductions in light-duty vehicle energy use and greenhouse gas emissions. Massachusetts Institute of Technology, 2015.

[3] Husted, H. L. Flexible electrified powertrains for today and tomorrow. Hyundai-Kia International Powertrain Conference, 2018.

[4] Sunde, E. Powertrain outlook electrification, engines & transmissions 2017-2025. Detroit Assn. of Business Economists/Wards Intelligence Conference, 2018.

[5] Grimm, J. Managing the transformation of powertrain. Hyundai-Kia International Powertrain Conference, 2018.

[6] The french automotive industry, analysis & statistics 2018. The Comité des Constructeurs Français d'Automobiles, 2018.

[7] Heywood, J. B. Internal combustion engine fundamentals. 1988.

[8] Nates, R. and Yates, A. Knock damage mechanisms in spark-ignition engines. *SAE International Journal of Fuels and Lubricants* 103 (1994): 1970-80.

[9] Fitton, J. and Nates, R. Knock erosion in spark-ignition engines. SAE Technical Paper 962102, 1996.

[10] Wang, Z., Liu, H., Song, T., Qi, Y., He, X., Shuai, S. and Wang, J. Relationship between super-knock and pre-ignition. *International Journal of Engine Research* 16, no. 2 (2015): 166-80.

[11] Wang, Z., Liu, H. and Reitz, R. D. Knocking combustion in spark-ignition engines. *Progress in Energy Combustion Science* 61 (2017): 78-112.

[12] Ham, Y. Y., Chun, K. M., Lee, J. H. and Chang, K. S. Spark-ignition engine knock control and threshold value determination. SAE Technical Paper 960496, 1996.

[13] Stotsky, A. A. Statistical engine knock modelling and adaptive control. *Proceedings of the Institution of Mechanical Engineers, Part D: Journal of Automobile Engineering* 222, no. 3 (2008): 429-39.

[14] Zhu, G., Haskara, I. and Winkelman, J. "Stochastic limit control and its application to spark limit control using ionization feedback." Paper presented at the American Control Conference, 2005. Proceedings of the 2005, 2005.

[15] Thomasson, A., Shi, H., Lindell, T., Eriksson, L., Shen, T. and Jones, J. C. P. Experimental validation of a likelihood-based stochastic knock controller. *IEEE Transactions on Control Systems Technology* 24, no. 4 (2016): 1407-18.

[16] Turns, S. R. An introduction to combustion: Concepts and applications 1999.

[17] Zhen, X., Wang, Y., Xu, S., Zhu, Y., Tao, C., Xu, T. and Song, M. The engine knock analysis–an overview. *Applied Energy* 92 (2012): 628-36.

[18] McKenzie, J. and Cheng, W. K. The anatomy of knock. SAE Technical Paper 2016-01-0704, 2016.

[19] Douaud, A. and Eyzat, P. Four-octane-number method for predicting the anti-knock behavior of fuels and engines. SAE Technical Paper 780080, 1978.

[20] Chen, L., Li, T., Yin, T. and Zheng, B. A predictive model for knock onset in spark-ignition engines with cooled egr. *Energy Conversion Management* 87 (2014): 946-55.

[21] Soylu, S. Prediction of knock limited operating conditions of a natural gas engine. *Energy Conversion and Management* 46, no. 1 (2005): 121-38.

[22] Livengood, J. and Wu, P. "Correlation of autoignition phenomena in internal combustion engines and rapid compression machines." Paper presented at the Symposium (international) on combustion, 1955.

[23] He, X., Donovan, M., Zigler, B., Palmer, T., Walton, S., Wooldridge, M. and Atreya, A. An experimental and modeling study of iso-octane ignition delay times under homogeneous charge compression ignition conditions. *Combustion and Flame* 142, no. 3 (2005): 266-75.

[24] He, X., Qi, Y., Wang, Z., Wang, J., Shuai, S. and Tao, L. Visualization of the mode shapes of pressure oscillation in a cylindrical cavity. *Combustion Science and Technology* 187, no. 10 (2015): 1610-19.

[25] Worret, R., Bernhardt, S., Schwarz, F. and Spicher, U. Application of different cylinder pressure based knock detection methods in spark ignition engines. SAE Technical Paper 2002-01-1668, 2002.

[26] Hoepke, B., Jannsen, S., Kasseris, E. and Cheng, W. K. Egr effects on boosted si engine operation and knock integral correlation. *SAE International Journal of Engines* 5, no. 2 (2012): 547-59.

[27] McKenzie, J. and Cheng, W. K. Ignition delay correlation for engine operating with lean and with rich fuel-air mixtures. SAE Technical Paper 2016-01-0699, 2016.

[28] Cho, S. Study on the efffect of cylinder wall temperatures on knock characteristics in spark-ignited engine. Seoul National University, 2018.

[29] Kalghatgi, G., Algunaibet, I. and Morganti, K. On knock intensity and superknock in si engines. *SAE International Journal of Engines* 10, no. 2017-01-0689 (2017): 1051-63.

[30] Borg, J. M. and Alkidas, A. C. Cylinder-pressure-based methods for sensing spark-ignition engine knock. *International Journal of vehicle design* 45, no. 1-2 (2007): 222-41.

[31] Xiaofeng, G., Stone, R., Hudson, C. and Bradbury, I. The detection and quantification of knock in spark ignition engines. SAE Technical Paper 932759, 1993.

[32] Hudson, C., Gao, X. and Stone, R. Knock measurement for fuel evaluation in spark ignition engines. *Fuel* 80, no. 3 (2001): 395-407.

[33] Brecq, G., Bellettre, J. and Tazerout, M. A new indicator for knock detection in gas si engines. *International Journal of Thermal Sciences* 42, no. 5 (2003): 523-32.

[34] Shahlari, A. J. and Ghandhi, J. Pressure-based knock measurement issues. SAE Technical Paper 2017-01-0668, 2017.

[35] Lee, J.-H., Hwang, S.-H., Lim, J.-S., Jeon, D.-C. and Cho, Y.-S. A new knock-detection method using cylinder pressure, block vibration and sound pressure signals from a si engine. SAE Technical Paper 981436, 1998.

[36] Kim, K. S. Study of engine knock using a monte carlo method. The University of Wisconsin-Madison, 2015.

[37] Nakata, K., Nogawa, S., Takahashi, D., Yoshihara, Y., Kumagai, A. and Suzuki, T. Engine technologies for achieving 45% thermal efficiency of si engine. *SAE International Journal of Engines* 9, no. 1 (2016): 179-92.

[38] Matsuo, S., Ikeda, E., Ito, Y. and Nishiura, H. The new toyota inline 4 cylinder 1.8 l estec 2zr-fxe gasoline engine for hybrid car. SAE Technical Paper 2016-01-0684, 2016.

[39] Lee, B., Oh, H., Han, S., Woo, S. and Son, J. Development of high efficiency gasoline engine with thermal efficiency over 42%. SAE Technical Paper 2017-01-2229, 2017.

[40] Hwang, K., Hwang, I., Lee, H., Park, H., Choi, H., Lee, K., Kim, W., Kim, H., Han, B. and Lee, J. Development of new high-efficiency kappa 1.6 l gdi engine. SAE Technical Paper 2016-01-0667, 2016.

[41] Shibata, M., Komatsu, H., Maeyama, K., Asari, M., Hotta, N., Nakada, K. and Daicho, H. New 1.0 l i3 turbocharged gasoline direct injection engine. SAE Technical Paper 2017-01-1029, 2017.

[42] Takahashi, D., Nakata, K. and Yoshihara, Y. Engine thermal control for improving the engine thermal efficiency and anti-knocking quality. SAE Technical Paper 2012-01-0377, 2012.

[43] Imaoka, Y., Shouji, K., Inoue, T. and Noda, T. A study of combustion technology for a high compression ratio engine: The influence of combustion chamber wall temperature on knocking. *SAE International Journal of Engines* 9, no. 2 (2016): 768-76.

[44] Schenk, M., Schröter, F., Zellinger, F., Klaus, B., Pfeiffer, D. and Fischer, H. "Corona-ignition vs. Spark ignition: A fundamental comparison for varying thermodynamic conditions of modern turbocharged gasoline engines." Paper presented at the International Conference: SIA Powertrain, Versailles, 2015.

[45] Krüger, P., Visser, B. and Mackenzie, J. Advanced plasma and variable spark ignition system. *IAV 2nd Ignition Converence, Berlin* (2014).

[46] Hese, M., Tschöke, H., Breuninger, T., Altenschmidt, F. and Winter, H. Influence of a multispark ignition system on the inflammation in a spray-guided combustion process. *SAE International Journal of Fuels and Lubricants* 2, no. 2 (2010): 376-86.

[47] Cavina, N., Corti, E., Poggio, L. and Zecchetti, D. Development of a multi-spark ignition system for reducing fuel consumption and exhaust emissions of a high performance gdi engine. SAE Technical Paper 2011-01-1419, 2011.

[48] Yoshihara, Y., Nakata, K., Takahashi, D., Omura, T. and Ota, A. Development of high tumble intake-port for high thermal efficiency engines. SAE Technical Paper 2016-01-0692, 2016.

[49] Omura, T., Nakata, K., Yoshihara, Y. and Takahashi, D. Research on the measures for improving cycle-to-cycle variations under high tumble combustion. SAE Technical Paper 2016-01-0694, 2016.

[50] Morita, T., Hidaka, T. and Kashimura, Y. System and method for controlling ignition timing for an internal combustion engine. Patent, US4819603A.

[51] Cho, H., Lee, J. and Yoo, J. A study of the adaptive control of spark timing using cylinder pressure in a spark ignition engine. *Proceedings of the Institution of Mechanical Engineers, Part D: Journal of Automobile Engineering* 213, no. 5 (1999): 435-40.

[52] Cho, H., Lee, K., Lee, J., Yoo, J. and Min, K. Measurements and modeling of residual gas fraction in si engines. SAE Technical Paper 2001-01-1910, 2001.

[53] Ford, R., Collings, N. and Collins, N. Measurement of residual gas fraction using a fast response no sensor. *SAE International Journal of Engines* 108 (1999): 258-67.

[54] Giansetti, P., Perrier, C., Higelin, P., Chamaillard, Y., Charlet, A. and Couet, S. A model for residual gas fraction prediction in spark ignition engines. SAE Technical Paper 2002-01-1735, 2002.

[55] Karagiorgis, S., Collings, N., Glover, K., Coghlan, N. and Petridis, A. Residual gas fraction measurement and estimation on a homogeneous charge compression ignition engine utilizing the negative valve overlap strategy. SAE Technical Paper 2006-01-3276, 2006.

[56] Fox, J., Cheng, W. and Heywood, J. A model for predicting residual gas fraction in spark-ignition engines. *SAE International Journal of Engines* (1993).

[57] Senecal, P., Xin, J. and Reitz, R. D. Predictions of residual gas fraction in ic engines. SAE Technical Paper 962052, 1996.

[58] Mladek, M. and Onder, C. H. A model for the estimation of inducted air mass and the residual gas fraction using cylinder pressure measurements. SAE Technical Paper 2000-01-0958, 2000.

[59] Cavina, N., Siviero, C. and Suglia, R. Residual gas fraction estimation: Application to a gdi engine with variable valve timing and egr. SAE Technical Paper 2004-01-2943, 2004.

[60] Kale, V., Yeliana, Y., Worm, J. and Naber, J. Development of an improved residuals estimation model for dual independent cam phasing spark-ignition engines. SAE Technical Paper 2013-01-0312, 2013.

[61] Eriksson, L. and Andersson, I. An analytic model for cylinder pressure in a four stroke si engine. SAE Technical Paper 2002-01-0371, 2002.

[62] Lee, Y. and Min, K. Prediction of polytropic index during compression stroke in diesel engine. Korean Society of Automotive Engineers Fall Conference, 2018.

[63] Lee, S. Modeling of a real-time virtual pressure and nox sensor for light-duty diesel engines. Seoul National University, 2017.

[64] Bonatesta, F., Waters, B. and Shayler, P. Burn angles and form factors for wiebe function fits to mass fraction burned curves of a spark ignition

engine with variable valve timing. *International Journal of Engine Research* 11, no. 2 (2010): 177-86.

국 문 초 록

가솔린 엔진의 효율 향상은 지속적으로 연구되어 왔으나, 최근의 급격히 강화되는 연비, 배기 규제로 인해 효율 향상의 필요성이 그 어느 때보다 더욱 대두되고 있다. 따라서 가솔린 엔진의 효율 향상을 위한 다양한 방법이 제시되고 있으며, 그 중에서도 압축비의 상승은 효율 개선에 매우 효과적이다. 그러나 압축비의 상승은 혼합기의 초기 온도를 상승시키며, 이는 연소기간 중 말단가스의 온도 상승으로 직결되어 미연 가스의 자발화 현상이 발생하기 쉽게 한다.

자발화 현상이 폭발의 형태로 발생하는 경우, 순간적인 열 방출이 발생하고 실린더 내부에 압력파를 형성하여 소음과 엔진 손상을 유발한다. 이는 노킹 현상으로 불리며, 엔진 손상을 방지하기 위하여 반드시 회피되어야 한다. 따라서 이에 대해 노킹을 저감하는 연구뿐만 아니라, 노킹을 회피하기 위한 다양한 제어 알고리즘이 제시되고 있다.

기존 양산 차량에서의 노킹 제어 알고리즘은 노킹 센서에 의존하고 있으며, 이는 센서에서 노킹 발생을 감지하는 것이 선행되어야 하므로 노킹을 완전히 회피할 수 없다. 또한, 노킹 발생 시 회피를 위해 제어인자가 급격히 변경되며, 이는 운전편의성이 나빠질 뿐만 아니라, 엔진 효율을 감소시키게 된다. 이러한 점을 개선하기 위해 제어인자를 점진적으로 변경하는 등 진보적인 제어 방법이 개발되고 있다.

노킹현상은 엔진 내의 유동, 열 전달 및 연소 특성과 같은 인자에 영향을 받으므로, 무작위적인 특성을 보인다. 따라서, 노킹을 보수적으로 회피하기 위해 기존의 제어는 노킹 회피 후에 운전 인자를 천천히 최적 운전 조건으로 복귀시킨다. 이는 전반적으로

효율이 낮은 지점에 운전 조건을 유지시키므로, 이를 개선한다면 고부하 조건에서 추가적인 효율 상승을 기대할 수 있다.

이에 대한 개선 방법의 하나로 노킹을 예측하여 선재적으로 제어를 수행하는 모델 기반의 제어를 제시할 수 있다. 이 경우, 노킹을 회피하기 용이해 질 뿐만 아니라, 노킹 발생 사전에 제어 인자를 지정함으로써 기존에 발생하던 과도한 제어 인자 변경으로 인한 효율 저하를 방지할 수 있다.

본 연구에서는 선재적 제어를 위한 기저연구로, 엔진에서의 노킹 발생 예측에 대한 모델링이 이루어졌다. 모델에는 실제 운전 상황에의 적용을 고려하여, 기존 양산 엔진에서 얻을 수 있는 변수 및 측정값만이 이용되었다. 첫째로, 실린더 내 압력 예측 모델링이 이루어 졌으며, 이는 실린더 내부 초기 조건의 판정, 압축기간 동안의 압력 예측, 그리고 연소율을 이용한 연소 압력 예측의 세가지 과정으로 진행되었다.

둘째로, 예측된 압력을 이용하여 미연가스의 온도를 계산하였으며, 이는 점화 지연을 계산하는 데에 이용되었다. 점화 지연은 실제 자발화 발생 여부를 판정하지 못하므로, 예측된 자발화 시점에서의 연소율을 이용하여 노킹 여부를 판정하였다. 구성된 모델은 사이클 별 편차가 고려된 압력 예측모델과 함께 적용되었을 경우 노킹 발생 빈도를 잘 예측하여, 충분한 예측 정확성을 가지고 있다고 판단되었다.

주요어: 가솔린 엔진, 노킹 예측, 실린더 압력 예측, 자발화, 점화 지연

학 번: 2017-29399